

Article

# Stereodivergent Protein Engineering of a Lipase to Access All Possible Stereoisomers of Chiral Esters with Two Stereo-centers

Jian Xu, Yixin Cen, Warispreet Singh, Jiajie Fan, Lian Wu, Xianfu Lin, Jiahai Zhou, Meilan Huang, Manfred T. Reetz, and Qi Wu

*J. Am. Chem. Soc.*, **Just Accepted Manuscript** • DOI: 10.1021/jacs.9b02709 • Publication Date (Web): 26 Apr 2019

Downloaded from <http://pubs.acs.org> on April 26, 2019

## Just Accepted

"Just Accepted" manuscripts have been peer-reviewed and accepted for publication. They are posted online prior to technical editing, formatting for publication and author proofing. The American Chemical Society provides "Just Accepted" as a service to the research community to expedite the dissemination of scientific material as soon as possible after acceptance. "Just Accepted" manuscripts appear in full in PDF format accompanied by an HTML abstract. "Just Accepted" manuscripts have been fully peer reviewed, but should not be considered the official version of record. They are citable by the Digital Object Identifier (DOI®). "Just Accepted" is an optional service offered to authors. Therefore, the "Just Accepted" Web site may not include all articles that will be published in the journal. After a manuscript is technically edited and formatted, it will be removed from the "Just Accepted" Web site and published as an ASAP article. Note that technical editing may introduce minor changes to the manuscript text and/or graphics which could affect content, and all legal disclaimers and ethical guidelines that apply to the journal pertain. ACS cannot be held responsible for errors or consequences arising from the use of information contained in these "Just Accepted" manuscripts.



ACS Publications

is published by the American Chemical Society, 1155 Sixteenth Street N.W., Washington, DC 20036

Published by American Chemical Society. Copyright © American Chemical Society. However, no copyright claim is made to original U.S. Government works, or works produced by employees of any Commonwealth realm Crown government in the course of their duties.

# Stereodivergent Protein Engineering of a Lipase to Access All Possible Stereoisomers of Chiral Esters with Two Stereocenters

Jian Xu,<sup>†,‡</sup> Yixin Cen,<sup>†,||,‡</sup> Warispreet Singh,<sup>§</sup> Jiajie Fan,<sup>†</sup> Lian Wu,<sup>||</sup> Xianfu Lin,<sup>†</sup> Jiahai Zhou,<sup>||,\*</sup>, Meilan Huang,<sup>§,\*</sup> Manfred T. Reetz,<sup>||,#,\*</sup> & Qi Wu<sup>†,\*</sup>

<sup>†</sup>Department of Chemistry, Zhejiang University, Hangzhou, 310027, P. R. China;

<sup>§</sup>School of Chemistry and Chemical Engineering, Queen's University, David Keir Building, Stranmillis Road, Belfast BT9 5AG, Northern Ireland, UK;

<sup>||</sup>State Key Laboratory of Bio-organic and Natural Products Chemistry, Shanghai Institute of Organic Chemistry, Chinese Academy of Sciences, Shanghai 200032, China;

<sup>¶</sup>Max-Planck-Institut für Kohlenforschung, Kaiser-Wilhelm-Platz 1, 45470, Mülheim an der Ruhr, Germany.

<sup>#</sup>Chemistry Department, Philipps-University, Hans-Meerwein-Str. 4, 35032 Marburg, Germany.

**KEYWORDS.** *lipases; directed evolution; stereodivergent protein engineering; multiple stereocenters; solvent effects.*

**ABSTRACT:** Enzymatic stereodivergent synthesis to access all possible product stereoisomers bearing multiple stereocenters is relatively undeveloped, although enzymes are being increasingly used in both academic and industrial areas. When two stereocenters and thus four stereoisomeric products are involved, obtaining stereodivergent enzyme mutants for individually accessing all four stereoisomers would be ideal. Although significant success has been achieved in directed evolution of enzymes in general, stereodivergent engineering of one enzyme into four highly stereocomplementary variants for obtaining the full complement of stereoisomers bearing multiple stereocenters remains a challenge. Using *Candida antarctica* lipase B (CALB) as a model, we report the protein engineering of this enzyme into four highly stereocomplementary variants needed for obtaining all four stereoisomers in transesterification reactions between racemic acids and racemic alcohols in organic solvents. By generating and screening less than 25 variants each isomer, we achieved >90% selectivity for all of the four possible stereoisomers in the model reaction. This difficult feat was accomplished by developing a strategy dubbed “focused rational iterative site-specific mutagenesis” (FRISM) at sites lining the enzyme’s binding pocket. The accumulation of single mutations by iterative site-specific mutagenesis using a restricted set of rationally chosen amino acids allows the formation of ultra-small mutant libraries requiring minimal screening for stereoselectivity. The crystal structure of all stereodivergent CALB variants, flanked by MD simulations, uncovered the source of selectivity.

## INTRODUCTION

Different enantiomers of a biologically active molecule generally have different physiological properties, such as different degree or different type of biological activities, or even opposite bioactivity or toxic side effects.<sup>1</sup> One of the most representative examples is thalidomide, which has been cited many times in discussions of this kind.<sup>1,2</sup> The relationship between the chirality of molecules and their bioactivity becomes substantially more complex when compounds contain multiple stereocenters. For example, (2*R*, 3*R*)-pachlobutrazol is a fungicide, while (2*S*, 3*S*)- pachlobutrazol is a plant growth regulator.<sup>3</sup> The (*S*, *S*)-form of ethambutol is a front-line anti-tuberculosis drug, while the (*R,R*)-enantiomer is completely inactive against mycobacterium tuberculosis, and the (*R*, *S*)-diastereomer is 16 times less effective.<sup>4</sup> Thus, it is necessary to have easy access to all theoretically possible stereoisomers of a drug candidate in order to evaluate their bioactivity carefully. Despite remarkable progress in the field of asymmetric synthesis over the past few decades,<sup>5</sup> complete

control of multiple stereogenic centers for obtaining all possible stereoisomers in catalyst-controlled reactions remains a challenge.

Asymmetric transformations such as desymmetrization of meso-epoxides by Jacobsen-catalysts allow access to both of the expected enantiomers, but not to the respective diastereomers.<sup>6</sup> Some well-designed man-made catalysts for stereodivergent synthesis methods have emerged which allow access to some and in rare cases even all stereoisomeric products with multiple stereocenters from the same set of precursors. For example, Carreira and coworkers described the fully stereodivergent synthesis of  $\gamma,\delta$ -unsaturated aldehydes bearing two vicinal quaternary/tertiary stereogenic centers by an ingenious dual catalytic procedure based on a chiral Ir-catalyst and a chiral amine co-catalyst for accessing all four stereoisomers.<sup>7</sup> In a different and likewise impressive approach, Buchwald and co-workers recently demonstrated the synthesis of all stereoisomers of a set of 1,3-amino alcohols bearing up to three contiguous stereocenters through

sequential, copper-hydride-catalyzed hydrosilylation and hydroamination of readily available enals and enones.<sup>8</sup> Diverse reviews have appeared describing asymmetric catalysis in which more than one stereocenter is involved.<sup>9</sup>

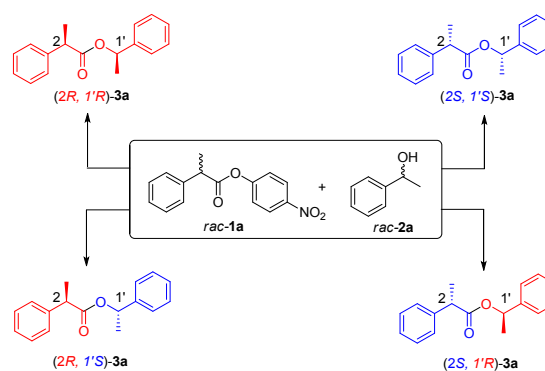
Enzymatic stereodivergent synthesis for accessing all possible stereoisomers bearing multiple stereocenters is a relatively undeveloped domain, although biocatalysts are being increasingly used in both academic and industrial laboratories.<sup>10</sup> For example, hydrolytic desymmetrization of meso-epoxides catalyzed by epoxide hydrolases allows entry into the two enantiomeric products, but generally not to the diastereomers.<sup>11</sup> The general problem may be due to the exquisite selectivity of enzymes, which usually causes limited substrate acceptance and access to only one of the possible stereoisomeric products. An alternative method utilizes tandem reactions, in which several enzymes sequentially control different stereocenters of products.<sup>12–13</sup> For example, we recently reported the combination of P450-BM3 mutants and appropriate alcohol dehydrogenases as catalysts in 4-step cascade reactions starting from cyclohexane leading optionally to either (*R,R*)-, (*S,S*)-, or (*R,S*)-cyclohexane-1,2-diols.<sup>12</sup> This was achieved by applying directed evolution using the combinatorial active-site saturation test (CAST) and iterative saturation mutagenesis (ISM) at residues lining the binding pocket.<sup>14</sup> However, developing a simple and rapid method based on a *single* enzyme for the complete control of absolute and relative configuration of products having multiple stereogenic centers and with selective formation of all theoretically possible stereoisomers represents a synthetic challenge in asymmetric biocatalysis.

Whereas stereocomplementary enzymes with formation of products having single stereocenters exist in nature<sup>15</sup> or can be evolved by directed evolution,<sup>14,16</sup> it is unlikely that those with divergent stereoselectivity leading to four different products with two stereogenic centers on an optional basis will be found without turning to mutagenesis.<sup>10</sup> In principle, several different reaction types can be considered in order to obtain products having two newly created stereogenic centers, mediated either by enzymes or man-made catalysts. For example, in P450-BM3 catalyzed desymmetrization of appropriate achiral compounds (or meso-compounds) such as methylcyclohexane with formation of 1-hydroxy-2-methylcyclohexane, only one of the four stereoisomers proved to be accessible by directed evolution.<sup>17</sup> A different reaction type is cyclopropanation of styrene, e.g., catalyzed by mutant Fe-heme proteins, in which two out of the four possible stereoisomers could be produced with reasonable selectivity.<sup>18</sup> It is worth noting that for some substrates, all four possible stereoisomers in the cyclopropanation were also obtained by using three different enzymes.<sup>18a</sup> To the best of our knowledge, so far few precedents are available on the directed evolution of an enzyme for a stereodivergent reaction in which all four possible stereoisomeric products were accessed. Hilvert and coworkers reported the directed evolution of an artificial retroaldolase which was engineered for promiscuous Michael reactions leading optionally to four stereocomplementary products with 80–85% selectivities.<sup>19</sup> In this interesting process, CH-acidic Michael donors such as cyano acetic acid ethyl ester undergo rapid racemization prior to addition to prochiral  $\alpha$ ,  $\beta$ -unsaturated ketones.

With these challenges in mind, we considered a very different reaction class and enzyme type. It concerns the

stereodivergent protein engineering of a single wildtype (WT) lipase<sup>10</sup> into four highly stereocomplementary variants for transesterification reactions in organic solvents. *Candida antarctica* lipase B (CALB) was chosen as the model enzyme to be evolved, one of the most extensively used biocatalysts in both industrial and academic laboratories.<sup>10,20</sup> It has two binding pockets at the active site for the acid (acyl) and alcohol parts of ester substrates, respectively.<sup>20</sup> Based on previous protein engineering studies and structural knowledge of the two selectivity pockets of CALB,<sup>20b,21,22</sup> we envisioned that the respective selectivities determined by the acyl or alcohol-binding pockets of CALB could be combined to form four highly stereocomplementary variants that exert control over the transesterification reactions of racemic ester *rac*-1a and alcohol *rac*-2a in organic solvents (Scheme 1). This means that we aimed to perform the reactions with 50% conversion in a kind of kinetic resolution (KR).<sup>10,23</sup>

**Scheme 1. Stereodivergent Transacylation between 2-Phenylpropionic Acid *p*-Nitrophenyl Ester (*rac*-1a) and 1-Phenylethanol (*rac*-2a) Catalyzed by CALB Mutants.**



Although non-aqueous reaction conditions increase the difficulty of direction evolution, which has been rarely implemented,<sup>24a</sup> we succeeded in engineering the selectivities (exceeding 90%) for each of the four possible stereoisomers in the model reaction (Scheme 1) by screening less than 100 transformants. The achievement is based on a new protein engineering strategy which we call “*focused rational iterative site-specific mutagenesis*” (FRISM). As will be seen, it is a logical fusion of rational design and directed evolution.

## RESULTS AND DISCUSSION

**Creation of Ultra-Small Focused CALB Mutant Libraries for Screening in an Organic Solvent.** In contrast to lipase-catalyzed hydrolysis in aqueous medium, transacylation in an organic solvent can be used more widely, because of some specific advantages of nonaqueous enzymology, including the high solubility of organic substrates in organic solvents and the solvent-dependency of enzyme properties.<sup>25</sup> A special area of enzyme catalysis in non-aqueous media is dynamic kinetic resolution (DKR) of *sec*-alcohols or *sec*-amines.<sup>26</sup> To date, almost all protein engineering examples of lipases dealt with the hydrolysis of esters in an aqueous medium using high-throughput screening. An exception is the directed evolution of *Candida antarctica* lipase A (CALA) for enantioselective transacylation of *sec*-alcohols in organic solvents.<sup>24a</sup> It should be noted that the best mutants obtained from hydrolysis reactions may not perform equally well for transacylation in organic solvents, since non-negligible solvent dependency for enzyme selectivity has been

observed,<sup>27</sup> and even reversed enantioselectivity may occur when changing from water to organic solvents.<sup>27b-c</sup>

Since the solvent has a great effect on lipase-catalyzed KR, we first tested the activity and enantioselectivity of WT CALB (immobilized on acrylic resin) toward the model reaction in 8 different organic solvents at 37 °C. Unfortunately, WT CALB showed poor diastereoselectivity in all of the tested solvents, a mixture of (2*S*, 1'*R*)-**3a** and (2*R*, 1'*R*)-**3a** being the main products (Table S1). Considering the relatively high activity observed in isopropyl ether (IPE), this solvent was chosen for subsequent mutagenesis and screening steps.

The difficulty for transacylation-based screening in organic solvents lies in the laborious purification, lyophilization or immobilization of each mutant in a large or medium-sized library. Although a method for microtiter-plate screening in organic solvents has been reported, it was used for lyophilized enzymes and not tested for enantioselectivity.<sup>28</sup> A seminal method for screening in organic solvents using nickel-coated 96-well microtiter plates was reported by Bäckvall et al.<sup>24a</sup> Alternatively, in order to reduce the costs, time and labor in the screening step, we set out to devise a mutagenesis method that allows the rapid creation of ultra-small focused libraries of high-quality comprising only a few dozen mutants, and requiring minimal screening.

In order to reach this goal, we developed a strategy, in analogy to ISM,<sup>14</sup> called “focused rational iterative site-specific mutagenesis” (FRISM) (Fig. 1). Instead of generating focused saturation mutagenesis libraries at sites lining the binding pocket in an iterative manner using highly reduced amino acid alphabets as building blocks as in CAST/ISM<sup>14</sup> or in a manner based on the use saturation mutagenesis simultaneously at several residues employing one or two chosen amino acids as building blocks at each position<sup>24a-b</sup>, FRISM calls for rational decisions on the choice of a highly limited set of amino acids to be introduced at the chosen CAST sites by site-specific mutagenesis in an iterative manner. Saturation mutagenesis is not involved in this approach. Notice that each new collection of mutants in a FRISM step constitutes a mini-library, radically smaller in size than the focused libraries in traditional saturation mutagenesis.<sup>14</sup> Depending upon the particular enzyme and the catalytic parameter to be evolved,<sup>24</sup> different structure-based choices need to be made. In the present study, we focused primarily on the steric properties of the amino acids when applying site-specific mutagenesis, and made rational decisions in order to reshape selected domains in the CALB binding pocket iteratively for accepting sterically demanding substrates.

Firstly, the crystal structure of CALB (PDB ID: 1TCA)<sup>20b</sup> was viewed closely for choosing appropriate mutation residues. The active site of CALB is characterized by the catalytic triad Asp187-His224-Ser105, an oxyanion hole, and a binding pocket composed of two domains, one for the acyl-moiety of the ester and another for the alcohol-part, respectively. It was logical to assume that the amino acid residues around the active site of CAL-B are the most influential ones for improving stereoselectivity and activity, since many successful examples for manipulating these enzyme parameters genetically are based on CAST.<sup>14</sup>

Following a thorough analysis of the structure of the CALB active site into which we docked substrate **1a**, seven mutation sites were selected for generating the respective focused mini-library (Fig. 1C).

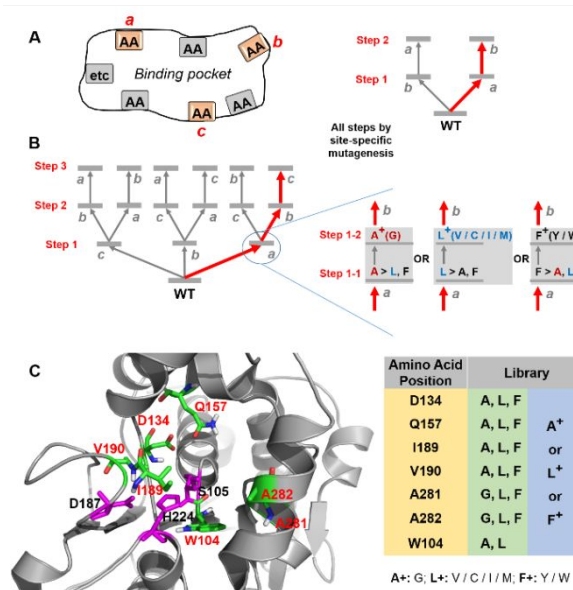


**Figure 1.** Representation of “focused rational iterative site-specific mutagenesis” (FRISM) and the X-ray structure of WT CALB.<sup>20b</sup> (A) Rationally identifying single amino acid (AA) residues for site specific mutagenesis. (B) FRISM based on 2 or 3 mutagenesis single sites, involving 2 or 6 upward pathways, respectively. (C) X-ray structure of WT CALB and amino acid residues included in the focused library. The residues of the catalytic triad Asp187-His224-Ser105 are shown in pink, and mutagenesis sites are shown in green/red stick illustrations. Alanine (A), leucine (L), and phenylalanine (F), regarded as small, medium and large amino acids, respectively. A<sup>+</sup>, L<sup>+</sup>, and F<sup>+</sup>, regarded as amino acids with similar steric properties used in the formation of extension libraries, including G, V/C/I/M and Y/W, respectively.

We then proceeded with FRISM in the following manner. A group of amino acids with different steric properties was chosen to replace the amino acids individually at the selected mutation sites: Alanine (A) or glycine (G), leucine(L), and phenylalanine(F) were regarded as small, medium and large amino acids, respectively, for modifying the space available in the two CALB binding pockets. Then, the obtained mutants were tested in the model reaction (Scheme 1) to identify the best key sites (“hotspots”) for manipulating stereoselectivity. This procedure is related to, but not identical to a strategy exploiting exploratory NNK-based SM at single residues lining the binding pocket, which enables rational decisions regarding the choice of reduced amino acid alphabets for further CAST/ISM at multi-residue randomization sites.<sup>14</sup> Since in the present case these simple exploratory experiments revealed some hits, a few additional mutations with similarly sized amino acids (A<sup>+</sup>, L<sup>+</sup> or F<sup>+</sup>) were then introduced individually at the key sites as an “extension-library” and screened for enhanced enantioselectivity. A<sup>+</sup>, L<sup>+</sup> and F<sup>+</sup> included G, V/C/I/M and Y/W, respectively.



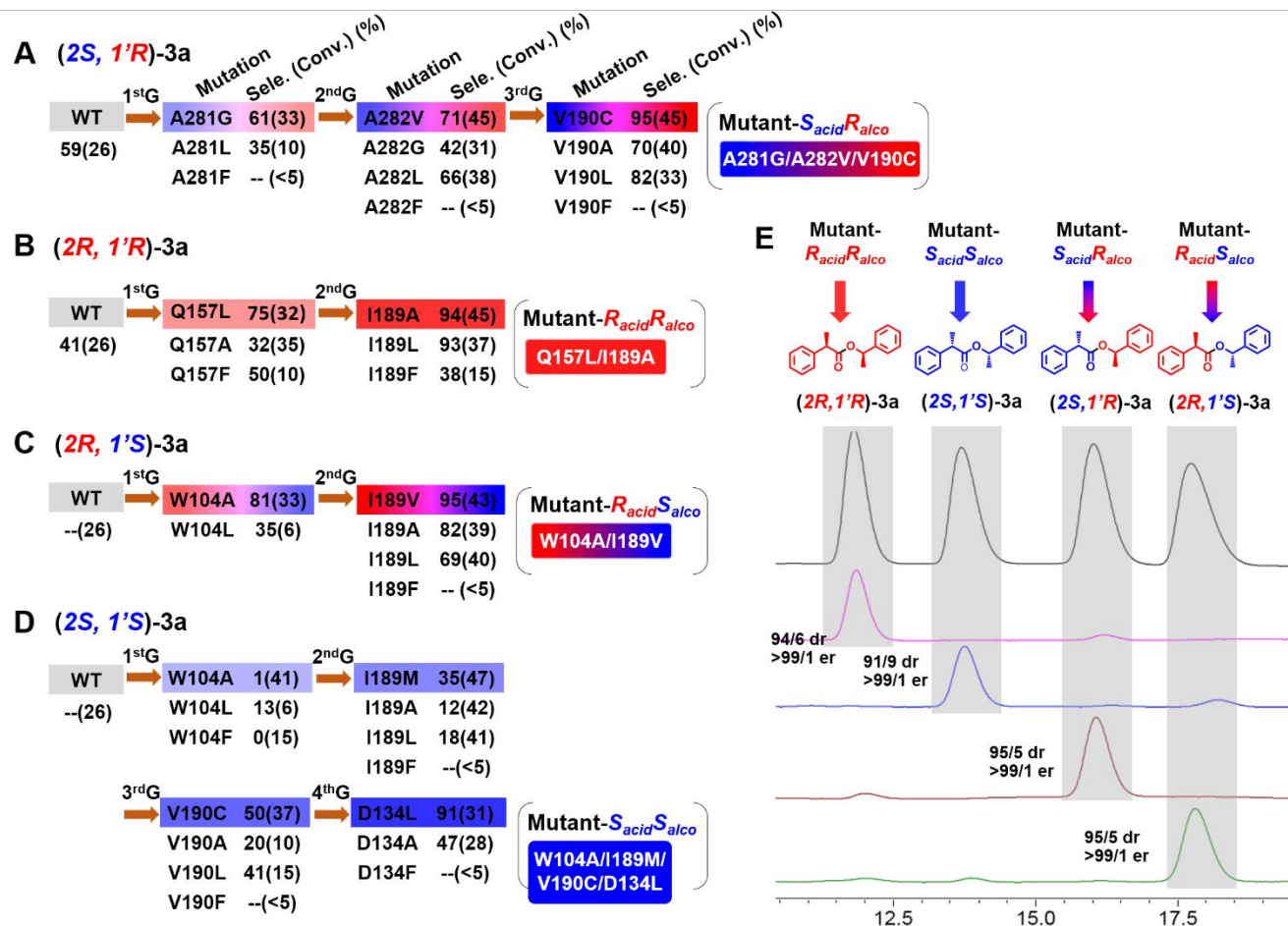


**Figure 2.** Focused rational iterative site-specific mutagenesis (FRISM) of CALB to obtain four enantioselective variants (A-D) as catalysts in the transacylation reactions between 2-phenylpropionic acid *p*-nitrophenyl ester (*rac*-1a) and 1-phenylethanol (*rac*-2a) providing four different enantio- and diastereomeric products 3a with diastereoselectivities ranging from 91:9 to 95:5 dr and enantioselectivities >99:1 er. Selectivity factors *E* are shown separately in Table 1. Abbreviations used: 1<sup>st</sup>-4<sup>th</sup> G: 1<sup>st</sup> to 4<sup>th</sup> generation of mutations; Sele.: selectivity, the percentage of the specific enantiomer in four different enantiomers of product 3a. Conversion data are shown in parentheses after the selectivity data of variants. HPLC conditions: OJ-H, hexane: isopropanol =80:20. The selectivity or percentage of four different enantiomers of product 3a in the model reaction catalyzed by various CALB mutants generated in the directed evolution process are listed in Table S2.

In the alcohol binding pocket, residue W104 is known to be an important site for manipulating the stereoselectivity of CALB toward racemic secondary alcohols.<sup>21a</sup> WT CALB displays excellent (*R*)-selectivity for many *sec*-alcohols, while some mutants such as W104A, first reported by Hult and coworkers,<sup>21a</sup> reverses enantioselectivity to (*S*). Therefore, the decision was made to explore directed evolution along two different routes.

In the first route, we kept W104 unchanged to maintain (*R*)-selectivity of CALB toward the alcohol part of the substrate, and then created a single library by modifying the acid-binding pocket for further manipulating the stereoselectivity toward the acid part of substrate 1a. Residues A281 and A282 were targeted by site-specific mutagenesis using amino acids A(A+), L(L+), and F(F+), respectively. Among the mutants of the first generation, A281G was the best mutant in favor of (2*S*, 1'*R*)-3a with a selectivity of 61% (Fig. 2A). In order to reverse enantioselectivity of the acid part, residue Q157, which occupies a large space and points to the oxyanion hole, was subjected individually to site-specific mutagenesis with

the introduction of A(A+), L(L+), and F(F+) mutations, respectively. To our satisfaction, in this small mutant collection, Q157L proved to be the best mutant which enhances reversed (*R*)-selectivity in favor of (2*R*, 1'*R*)-3a with 75% selectivity (Fig. 2B). As a consequence, we decided to use A281G and Q157L as the templates for further mutations at other chosen sites to improve the stereoselectivity of (2*S*, 1'*R*)-3a and (2*R*, 1'*R*)-3a, respectively.

In order to improve selectivity in favor of the (2*S*, 1'*R*)-3a enantiomer, the mutants of the second generation were generated by mutating A282 to G, L, and F. The screening results showed that A281G/A282L is the best mutant among this mini-library, improving selectivity from 61% to 66%. Further mutation of L+ amino acids at A282 position provided a better mutant, A281G/A282V with 71% selectivity in favor of (2*S*, 1'*R*)-3a (Fig. 2A). The same design was applied to the third position V190 which gives the third generation FRISM mutants. In this generation, the best mutant was found to be A281G/A282V/V190C, namely Mutant-*S*<sub>acid</sub>*R*<sub>alco</sub>, by pathway

281→282→190, with excellent selectivity (95/5 d.r.; >99/1 e.r) (Figs. 2A and 2E).

In order to improve the selectivity in the formation of (*R*<sub>acid</sub>,*R*<sub>alco</sub>)-**3a**, mutant Q157L was used as a template for iterative site-specific mutagenesis at other positions. I189 was first mutated according to the FRISM strategy. After screening this focused mini-library comprising I189A/L/F variants, Q157L/I189A (Mutant-*R*<sub>acid</sub>*R*<sub>alco</sub>) was identified as an excellent variant in the formation of (*R*<sub>acid</sub>,*R*<sub>alco</sub>)-**3a** (94/6 d.r.; >99/1 e.r) (Figs. 2B and 2E).

In the second route, W104 was first replaced by smaller amino acids to achieve (*S*)-selectivity toward the alcohol part of the substrate. A previous report had shown that mutation W104A induces only moderate (*S*)-selectivity in the acylation of 1-phenylethanol with vinyl butanoate (*E* = 6.6).<sup>21a</sup> We speculated that in our study W104A is not the only variant that could be useful. Therefore, we created a mini-library at position 104 containing A, L, and F mutations. To our surprise, in the formation of the (2*R*, 1'*S*)-**3a** enantiomer, (*R*)-selectivity of the acid part was improved significantly using either W104A or W104L. This shows that the modification of the alcohol pocket also alters the substrate binding mode in the acid pocket, indicating the occurrence of cooperative mutational effects.<sup>29</sup> The mutant W104A with moderate activity was then selected as the template for FRISM-based site-specific mutagenesis in order to further enhance (2*R*, 1'*S*)-**3a**-selectivity (Fig. 2C). It is worth noting that the selectivity manipulation in the formation of (2*S*, 1'*S*)-**3a** is much more difficult, because both W104A and W104L show very low selectivity for this particular absolute configuration (Fig. 2D).

For improving the selectivity of (2*R*, 1'*S*)-**3a**-formation, we therefore used the W104A-template and selected Q157 and I189 as the mutation points for the second generation FRISM. The choice of these CAST positions was made in view of their important effect on (*R*)-selectivity towards the acid motif of the substrate. Surprisingly, most tested mutations at Q157 including A, L, and F when added to W104A, caused a notable reduction of enzyme activity (data not shown), probably due to the destruction of the active site in these mutants. In contrast, the second generation FRISM mini-library with mutations at I189 introduced to the W104A template harbored an excellent mutant, W104A/I189V (Mutant-*R*<sub>acid</sub>*S*<sub>alco</sub>), showing high diastereoselectivity (95/5 d.r) and enantioselectivity (>99/1 e.r) in the formation of (2*R*, 1'*S*)-**3a** (Figs. 2C and 2E). In parallel work, the selective preference for (2*S*, 1'*S*)-**3a** was first observed with mutant W104A/I189M (35% selectivity, Fig. 2D) from the same second generation FRISM mini-library as Mutant-*R*<sub>acid</sub>*S*<sub>alco</sub>. Therefore, the decision was made to continue the evolutionary process using this mutant as the template to enhance selectivity in the production of (2*S*, 1'*S*)-**3a**, again by way of FRISM. Initially, this provided mutant W104A/I189M/V190C, which showed 50% selectivity for (2*S*, 1'*S*)-**3a**. The best mutant was discovered at the end of pathway 104→189→190→134. After screening this focused mini collection comprising D134A/L/F variants, W104A/I189M/V190C/D134L (91/9 d.r.; 99/1 e.r) was identified as the best mutant for the formation of (2*S*, 1'*S*)-**3a** enantiomer (Figs. 2D and 2E).

**Substrate Scope of the Evolved CALB Mutants.** Next, we wanted to see how the four best stereocomplementary mutants perform as catalysts in the transesterification of other

structurally different racemic acids and alcohols. We first tested these substrates with WT CALB (Table S3). Most WT CALB-catalyzed transesterification reactions provided mainly (2*R*, 1'*R*)- and (2*S*, 1'*R*)-diastereomers with very low d.r. values, and no (2*R*, 1'*S*)- or (2*S*, 1'*S*)-products were detected. As before, this is not unexpected, because WT CALB is known to display a remarkably high preference for (*R*)-*sec* alcohols and a relatively low stereoselectivity towards substrates with chirality centers in the acid part.<sup>21</sup> We also tested the performance of the four best stereocomplementary mutants in 6 different solvents (Table S4) where WT CALB showed different activity and selectivity. Of these solvents, isopropyl ether (IPE) was still the best choice for all the four best mutants. It is consistent with the result of WT CALB.

The four best stereocomplementary mutants display quite different results with regard to substrate acceptance and selectivity (Table 1). By using Mutant-*R*<sub>acid</sub>*R*<sub>alco</sub>, Mutant-*S*<sub>acid</sub>*R*<sub>alco</sub>, or Mutant-*R*<sub>acid</sub>*S*<sub>alco</sub>, respectively, a number of aromatic *p*-nitrophenol esters and *sec*-alcohols could be efficiently transformed to the corresponding chiral esters with remarkably enhanced stereoselectivity. For example, Mutant-*S*<sub>acid</sub>*R*<sub>alco</sub> has a broad substrate scope. In the acid domain of the target products with (2*S*, 1'*R*) configuration, different substituents on the phenyl ring, including methyl, halogen, isobutyl and different alkyl groups at the α-position such as methyl and ethyl are all tolerated. Similarly, in the *sec*-alcohol moiety of the tested substrates, heterocyclic structures and various substituents on the phenyl ring are also accepted. Remarkably, fatty *sec*-alcohol structures in the target products ((2*S*, 1'*R*)-**3f**, (2*S*, 1'*R*)-**3g**) are efficiently differentiated by Mutant-*S*<sub>acid</sub>*R*<sub>alco</sub>, while this cannot be achieved by WT CALB because it usually cannot differentiate between methyl and ethyl at the α-position of the *sec*-alcohol fragment of substrates.<sup>21</sup> Previous reports showed that WT-CALB has very low activity and selectivity in the KR of ibuprofen esters such as ibuprofen-PNP ester, which has a similar bulky ester group as (2*S*, 1'*R*)-**3r**.<sup>22b-c</sup> Notably, Mutant-*S*<sub>acid</sub>*R*<sub>alco</sub> also offers a very effective resolution for *rac*-ibuprofen, and high optical purity of the (2*S*, 1'*R*)-**3r** product can be obtained. Mutant-*S*<sub>acid</sub>*R*<sub>alco</sub> showed excellent stereoselectivity with 99/1 e.r. values, and moderate to high distereoselectivity with 64/36~97/3 d.r. for all the 18 compounds tested. Interestingly, Mutant-*S*<sub>acid</sub>*R*<sub>alco</sub> also retains good stereoselectivity in the conventional KR using substrate *rac*-**1a** alone or substrate *rac*-**2a** alone. For example, Mutant-*S*<sub>acid</sub>*R*<sub>alco</sub> provided the (*S*)-product with 21% yield and 99% ee in the transesterification of *rac*-**1a** and benzyl alcohol. Similarly, it can also provide (*R*)-product with 49% yield and 99% ee in the transesterification of *rac*-**2a** and vinyl acetate.

Compared with Mutant-*S*<sub>acid</sub>*R*<sub>alco</sub>, Mutant-*R*<sub>acid</sub>*R*<sub>alco</sub> has some notable differences in substrate scope. Methyl at the α-position of the acid section of the target compounds is accepted by Mutant-*R*<sub>acid</sub>*R*<sub>alco</sub>, but not ethyl. Moreover, contrary to Mutant-*S*<sub>acid</sub>*R*<sub>alco</sub>, fatty *sec*-alcohol structures in the targeted products ((2*R*, 1'*R*)-**3f** and (2*R*, 1'*R*)-**3g**) are not accepted by Mutant-*R*<sub>acid</sub>*R*<sub>alco</sub> (Table 1), probably due to the relative large space in the alcohol-binding pocket for small alkyl groups. Another interesting difference was observed in the formation of (2*R*, 1'*R*)-**3j** with 1-substituted

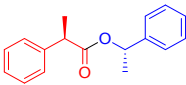
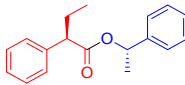
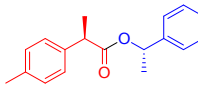
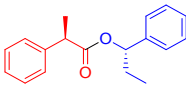
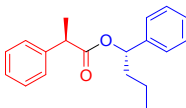
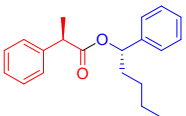
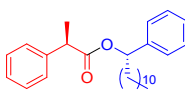
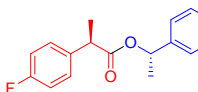
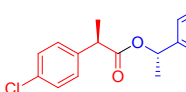
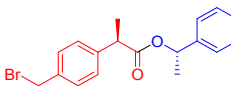
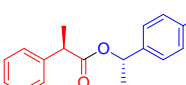
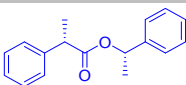
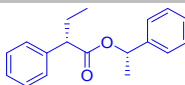
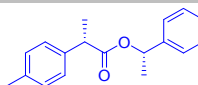
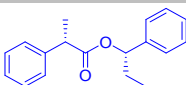
**Table 1. Substrate Scope of the Four Best FRISM-derived CALB Mutants as Catalysts in Stereoselective Reactions of *rac*-**

Esters and *rac*-Alcohols According to Scheme 1<sup>a</sup>.Mutant-*S*<sub>acid</sub>*R*<sub>alco</sub>

(2 <i>S</i> , 1' <i>R</i> )- <b>3a</b> , ton: 1246, yield: 45%, 95/5 d.r., >99/1 e.r. <i>E</i> <sub>major</sub> >200	(2 <i>S</i> , 1' <i>R</i> )- <b>3b</b> , ton: 851, yield: 42%, 95/5 d.r., <sup>b</sup> >99/1 e.r. <sup>c</sup> <i>E</i> <sub>major</sub> >200	(2 <i>S</i> , 1' <i>R</i> )- <b>3c</b> , ton: 425, yield: 31%, 90/10 d.r., >99/1 e.r. <i>E</i> <sub>major</sub> >200	(2 <i>S</i> , 1' <i>R</i> )- <b>3d</b> , ton: 1025, yield: 44%, 92/8 d.r., >99/1 e.r. <i>E</i> <sub>major</sub> >200	(2 <i>S</i> , 1' <i>R</i> )- <b>3e</b> , ton: 1201, yield: 43%, 83/17 d.r., >99/1 e.r. <i>E</i> <sub>major</sub> >200
(2 <i>S</i> , 2' <i>R</i> )- <b>3f</b> , ton: 1025, yield: 47%, 92/8 d.r., >99/1 e.r. <i>E</i> <sub>major</sub> >200	(2 <i>S</i> , 2' <i>R</i> )- <b>3g</b> , ton: 1210, yield: 49%, 97/3 d.r., >99/1 e.r. <i>E</i> <sub>major</sub> >200	(2 <i>S</i> , 1' <i>R</i> )- <b>3h</b> , ton: 814, yield: 41%, 88/12 d.r., >99/1 e.r. <i>E</i> <sub>major</sub> >200	(2 <i>S</i> , 1' <i>R</i> )- <b>3i</b> , ton: 941, yield: 44%, 97/3 d.r., >99/1 e.r. <i>E</i> <sub>major</sub> >200	(2 <i>S</i> , 1' <i>R</i> )- <b>3j</b> , ton: 910, yield: 41%, 64/36 d.r., >99/1 e.r. <i>E</i> <sub>major</sub> >200
(2 <i>S</i> , 1' <i>R</i> )- <b>3k</b> , ton: 954, yield: 45%, 91/9 d.r., >99/1 e.r. <i>E</i> <sub>major</sub> >200	(2 <i>S</i> , 1' <i>R</i> )- <b>3l</b> , ton: 514, yield: 35%, 78/22 d.r., >99/1 e.r. <i>E</i> <sub>major</sub> >200	(2 <i>S</i> , 1' <i>R</i> )- <b>3m</b> , ton: 1510, yield: 48%, 86/14 d.r., >99/1 e.r. <i>E</i> <sub>major</sub> >200	(2 <i>S</i> , 1' <i>R</i> )- <b>3n</b> , ton: 1025, yield: 48%, 89/11 d.r., >99/1 e.r. <i>E</i> <sub>major</sub> >200	(2 <i>S</i> , 1' <i>R</i> )- <b>3o</b> , ton: 1014, yield: 47%, 97/3 d.r., >99/1 e.r. <i>E</i> <sub>major</sub> >200
(2 <i>S</i> , 1' <i>R</i> )- <b>3p</b> , ton: 321, yield: 31%, 75/25 d.r., >99/1 e.r. <i>E</i> <sub>major</sub> >200	(2 <i>S</i> , 1' <i>R</i> )- <b>3q</b> , ton: 984, yield: 43%, 97/3 d.r., >99/1 e.r. <i>E</i> <sub>major</sub> >200	(2 <i>S</i> , 1' <i>R</i> )- <b>3r</b> , ton: 1012, yield: 45%, 92/8 d.r., >99/1 e.r. <i>E</i> <sub>major</sub> >200	( <i>S</i> )- <b>3v</b> , yield: 21%, 99.5/0.5 e.r. <i>E</i> <sub>major</sub> >200	( <i>R</i> )- <b>3w</b> , yield: 49%, 99.5/0.5 e.r. <i>E</i> <sub>major</sub> >200

Mutant-*R*<sub>acid</sub>*R*<sub>alco</sub>

(2 <i>R</i> , 1' <i>R</i> )- <b>3a</b> , ton: 987, yield: 45%, 94/6 d.r., >99/1 e.r. <i>E</i> <sub>major</sub> >200	(2 <i>R</i> , 1' <i>R</i> )- <b>3b</b> , n.d. <sup>d</sup>	(2 <i>R</i> , 1' <i>R</i> )- <b>3c</b> , ton: 457, yield: 32%, 89/11 d.r., >99/1 e.r. <i>E</i> <sub>major</sub> >200	(2 <i>R</i> , 1' <i>R</i> )- <b>3d</b> , ton: 458, yield: 34%, 92/8 d.r., >99/1 e.r. <i>E</i> <sub>major</sub> >200	(2 <i>R</i> , 1' <i>R</i> )- <b>3e</b> , ton: 594, yield: 35%, 86/14 d.r., >99/1 e.r. <i>E</i> <sub>major</sub> >200
(2 <i>R</i> , 2' <i>R</i> )- <b>3f</b> , n.d. <sup>d</sup>	(2 <i>R</i> , 2' <i>R</i> )- <b>3g</b> , n.d. <sup>d</sup>	(2 <i>R</i> , 1' <i>R</i> )- <b>3h</b> , ton: 531, yield: 38%, 75/25 d.r., 90/10 e.r. <i>E</i> <sub>major</sub> 15	(2 <i>R</i> , 1' <i>R</i> )- <b>3j</b> , ton: 458, yield: 35%, 97/3 d.r., 96/4 e.r. <i>E</i> <sub>major</sub> 39	(2 <i>R</i> , 1' <i>R</i> )- <b>3k</b> , ton: 621, yield: 41%, 67/33 d.r., >99/1 e.r. <i>E</i> <sub>major</sub> >200
(2 <i>R</i> , 1' <i>R</i> )- <b>3m</b> , ton: 686, yield: 42%, 97/3 d.r., >99/1 e.r.	(2 <i>R</i> , 1' <i>R</i> )- <b>3n</b> , ton: 1025, yield: 49%, 88/12 d.r., 94/6 e.r.	(2 <i>R</i> , 1' <i>R</i> )- <b>3o</b> , ton: 584, yield: 40%, 93/7 d.r., >99/1 e.r.	(2 <i>R</i> , 1' <i>R</i> )- <b>3p</b> , ton: 451, yield: 35%, 92/8 d.r., >99/1 e.r.	(2 <i>R</i> , 1' <i>R</i> )- <b>3q</b> , ton: 458, yield: 37%, 95/5 d.r., >99/1 e.r.

$E_{\text{major}} > 200$	$E_{\text{major}} 42$	$E_{\text{major}} > 200$	$E_{\text{major}} > 200$	$E_{\text{major}} > 200$
<b>Mutant-<math>R_{\text{acid}}S_{\text{alco}}</math></b>				
 (2 <i>R</i> , 1' <i>S</i> )- <b>3a</b> , ton: 968, yield: 43%, 95/5 d.r., >99/1 e.r. $E_{\text{major}} > 200$	 (2 <i>R</i> , 1' <i>S</i> )- <b>3b</b> , ton: 476, yield: 31%, 85/15 d.r., <sup>b</sup> 98/2 e.r. <sup>c</sup> $E_{\text{major}} 75$	 (2 <i>R</i> , 1' <i>S</i> )- <b>3c</b> , ton: 495, yield: 33%, 83/17 d.r., 97/3 e.r. $E_{\text{major}} 51$	 (2 <i>R</i> , 1' <i>S</i> )- <b>3d</b> , ton: 641, yield: 40%, 93/7 d.r., 98/2 e.r. $E_{\text{major}} 95$	 (2 <i>R</i> , 1' <i>S</i> )- <b>3s</b> , ton: 676, yield: 41%, 86/14 d.r., 96/4 e.r. $E_{\text{major}} 46$
 (2 <i>R</i> , 1' <i>S</i> )- <b>3t</b> , ton: 632, yield: 37%, 92/8 d.r., 98/2 e.r. $E_{\text{major}} 87$	 (2 <i>R</i> , 1' <i>S</i> )- <b>3u</b> , n.d. <sup>d</sup>	 (2 <i>R</i> , 1' <i>S</i> )- <b>3l</b> , ton: 351, yield: 29%, 80/20 d.r., 80/20 e.r. $E_{\text{major}} 5$	 (2 <i>R</i> , 1' <i>S</i> )- <b>3m</b> , ton: 632, yield: 32%, 94/6 d.r., <sup>b</sup> 98/2 e.r. <sup>c</sup> $E_{\text{major}} 77$	 (2 <i>R</i> , 1' <i>S</i> )- <b>3n</b> , ton: 1025, yield: 45%, 88/12 d.r., 96/4 e.r. $E_{\text{major}} 54$
 (2 <i>R</i> , 1' <i>S</i> )- <b>3o</b> , ton: 518, yield: 33%, 80/20 d.r., 97/3 e.r. $E_{\text{major}} 51$				
<b>Mutant-<math>S_{\text{acid}}S_{\text{alco}}</math></b>				
 (2 <i>S</i> , 1' <i>R</i> )- <b>3a</b> , ton: 751, yield: 31%, 91/9 d.r., >99/1 e.r. $E_{\text{major}} > 200$	 (2 <i>S</i> , 1' <i>R</i> )- <b>3b</b> , n.d. <sup>d</sup>	 (2 <i>S</i> , 1' <i>R</i> )- <b>3c</b> , ton: 432, yield: 25%, 71/29 d.r., 96/4 e.r. $E_{\text{major}} 32$	 (2 <i>S</i> , 1' <i>R</i> )- <b>3d</b> , ton: 311, yield: 21%, 78/22 d.r., <sup>b</sup> 94/6 e.r. <sup>c</sup> $E_{\text{major}} 20$	

<sup>a</sup> Reaction conditions: 50 mg immobilized lipase (10% enzyme on acrylic resin), *rac*-**1** (50 mM) and *rac*-**2** (45 mM) in 1 ml isopropyl ether at 37°C for 12 h. Yields and selectivity were determined by chiral HPLC. <sup>b</sup>d.r. was determined by NMR. <sup>c</sup>e.r. was determined by combining HPLC data and NMR. <sup>d</sup>n.d. not detected.

thiophene in the alcohol moiety, and of (2*R*, 1'*R*)-**3k** with 2-substituted thiophene. Mutant- $R_{\text{acid}}R_{\text{alco}}$  shows excellent distereoselectivity for (2*R*, 1'*R*)-**3j** (97/3 d.r.) and low selectivity for (2*R*, 1'*R*)-**3k**, while the result is exactly opposite to that of Mutant- $S_{\text{acid}}R_{\text{alco}}$ .

Mutant- $R_{\text{acid}}S_{\text{alco}}$  also shows good substrate scope. A series of (2*R*, 1'*S*)-esters with various substituents in the acid or alcohol moieties can be prepared with moderate to high d.r. and e.r. values. Especially,  $\alpha$ -alkyl groups with different chain length (from methyl to butyl) of the alcohol moiety ((2*R*, 1'*S*)-**3d**, **3s**, **3t**) are accepted by Mutant- $R_{\text{acid}}S_{\text{alco}}$ . However, when  $\alpha$ -alkyl was replaced by dodecyl, no activity was observed, implying that the substrate is too large to fit into the pocket. Mutant- $S_{\text{acid}}S_{\text{alco}}$  also increased the target selectivity of several

substrates. Relatively speaking, the substrate scope of Mutant- $S_{\text{acid}}S_{\text{alco}}$  is limited, which may be attributed to the specific active site structure of this mutant.

The reactions can be easily scaled up with good activity and selectivity, using (2*S*, 1'*R*)-**3a** and (2*S*, 1'*R*)-**3r** as two examples. The gram-scale reaction mixture containing 2.25 mmol **2a** and 2.5 mmol *rac*-**1a** (or *rac*-**1r**) under the catalysis of Mutant- $S_{\text{acid}}R_{\text{alco}}$  provides the corresponding (2*S*, 1'*R*)-**3a** with 37% isolated yield (211 mg), 96/4 d.r. and 99/1 e.r., and (2*S*, 1'*R*)-**3r** with 40% isolated yield (279 mg), 93/7 d.r. and 99/1 e.r., respectively. The ester group of the target products (e.g., (2*S*, 1'*R*)-**3r**) can be

**Table 2. Kinetic Data of WT CALB and Four Different Mutants<sup>a</sup>**



Substrate	(2 <i>R</i> , 1' <i>R</i> )-3a			(2 <i>R</i> , 1' <i>S</i> )-3a			(2 <i>S</i> , 1' <i>R</i> )-3a			(2 <i>S</i> , 1' <i>S</i> )-3a		
Mutant	$K_m$ (mM)	$k_{cat}$ (s <sup>-1</sup> )	$k_{cat}/K_m$ (M <sup>-1</sup> s <sup>-1</sup> )	$K_m$ (mM)	$k_{cat}$ (s <sup>-1</sup> )	$k_{cat}/K_m$ (M <sup>-1</sup> s <sup>-1</sup> )	$K_m$ (mM)	$k_{cat}$ (s <sup>-1</sup> )	$k_{cat}/K_m$ (M <sup>-1</sup> s <sup>-1</sup> )	$K_m$ (mM)	$k_{cat}$ (s <sup>-1</sup> )	$k_{cat}/K_m$ (M <sup>-1</sup> s <sup>-1</sup> )
WT	21.5	9.21	428	-	-	-	32.2	21.7	674	-	-	-
Mutant- <i>R</i> <sub>acid</sub> <i>R</i> <sub>alco</sub>	2.97	2.93	987	-	-	-	27.3	2.38	87.2	-	-	-
Mutant- <i>S</i> <sub>acid</sub> <i>R</i> <sub>alco</sub>	19.7	1.34	68.0	-	-	-	16.6	15.9	957	-	-	-
Mutant- <i>R</i> <sub>acid</sub> <i>S</i> <sub>alco</sub>	14.7	0.040	2.72	3.80	0.59	155	9.87	0.003	0.31	14.9	0.018	1.21
Mutant- <i>S</i> <sub>acid</sub> <i>S</i> <sub>alco</sub>	12.0	0.006	0.51	17.1	0.046	2.69	22.5	0.005	0.22	3.89	1.32	339

<sup>a</sup> Reaction conditions: 5mg immobilized lipase, *rac*-1a (3-40 mM) and *rac*-2a (100 mM) in 1 ml isopropyl ether at 37°C. Samples were taken at different reaction intervals for HPLC analysis.

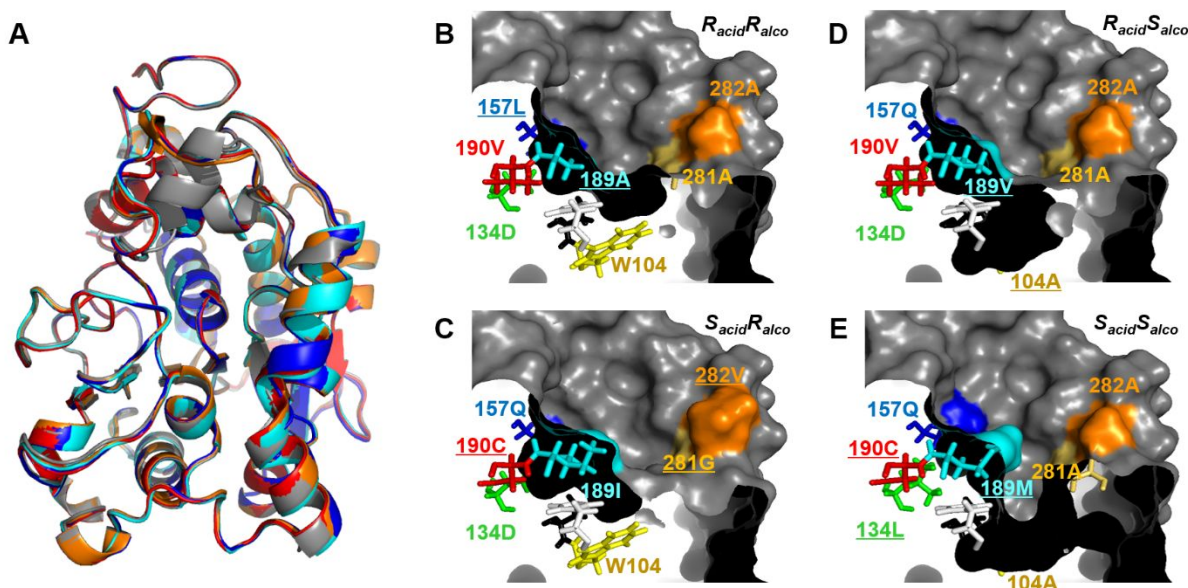


Figure 3. (A) Cartoon representation of the overall crystal structures of WT (PDB Code 5A71<sup>30</sup>, gray), Mutant- *R*<sub>acid</sub>*R*<sub>alco</sub> (PDB Code 6J1R, red), Mutant- *R*<sub>acid</sub>*S*<sub>alco</sub> (PDB Code 6J1Q, orange), Mutant- *S*<sub>acid</sub>*R*<sub>alco</sub> (PDB Code 6J1P, cyan), and Mutant- *S*<sub>acid</sub>*S*<sub>alco</sub> (PDB Code 6J1S, blue). Images B-E represent the surface of the binding pocket of these mutants (B: Mutant- *R*<sub>acid</sub>*R*<sub>alco</sub>; C: Mutant- *S*<sub>acid</sub>*R*<sub>alco</sub>; D: Mutant- *R*<sub>acid</sub>*S*<sub>alco</sub>; E: Mutant- *S*<sub>acid</sub>*S*<sub>alco</sub>). In images B-E, some representative residues are represented by sticks with different colors. S105 and H224 in B-E are colored in black and gray, respectively. All mutations in these four mutants are underlined.

easily hydrolyzed by using well-established methods, to give optical pure acids and alcohols simultaneously. This result also documents the synthetic utility of stereodivergent mutants of CALB in transesterification reactions.

These stereocomplementary mutants have largely retained thermostability relative to WT CALB. The measured  $T_{50}$  value of WT CALB (58.6 °C) and those of the four Mutants *R*<sub>acid</sub>*R*<sub>alco</sub> (55.7 °C), *S*<sub>acid</sub>*R*<sub>alco</sub> (59.2 °C), *R*<sub>acid</sub>*S*<sub>alco</sub> (53.6 °C) and *S*<sub>acid</sub>*S*<sub>alco</sub> (51.3 °C) suggest that the evolved mutations responsible for manipulated stereoselectivity do not impair the thermostability of the enzyme to any significant degree.

**Deconvolution Experiments.** In order to explore the effect of each amino acid exchange in the four best variants on the specific selectivity for the transesterification of 2-phenyl propionic acid *p*-nitrophenyl ester (1a) and 1-phenylethanol (2a), partial deconvolution of the four best

variants was performed. This was achieved by applying site-directed mutagenesis on WT CALB with creation of a select series of variants (Table S5).

For Mutant-*S*<sub>acid</sub>*R*<sub>alco</sub>, three single mutations and the double mutations derived from their combination proved to be ineffective in improving the (2*S*, 1'*R*)-selectivity relative to WT, while the triple mutant (V190C/A281G/A282V) was found to display 95% selectivity toward (2*S*, 1'*R*)-enantiomer, showing a remarkable synergistic effect<sup>29</sup> (Table S5, entries 1-7). Similar cooperative effects were also found in Mutant-*S*<sub>acid</sub>*S*<sub>alco</sub>, where all deconvoluted mutants showed low or even no preference for the (2*S*, 1'*S*)-enantiomer, while in concert their assembly showed 91% selectivity for the target enantiomer (Table S5, entries 14-27). It is also worth noting that in Mutant-*R*<sub>acid</sub>*S*<sub>alco</sub>, the mutation of W104A in the alcohol-binding pocket resulted in a

significant improvement of (2*R*, 1'*S*)-selectivity (Table S5, entry 11), completely reversing the (2*S*, 1'*R*)-preference of WT CALB. This result speaks for “remote” mutational effects.

**Kinetic Studies.** Kinetic parameters were measured for WT-CALB and the four stereocomplementary mutants (Table 2). It is noteworthy that WT-CALB has similar activity ( $k_{\text{cat}}/K_m$ ) towards the stereoisomers of (2*R*, 1'*R*)-**3a** and (2*S*, 1'*R*)-**3a**, whereas very low activity was determined in the case of (2*R*, 1'*S*)-**3a** and (2*S*, 1'*S*)-**3a**. The high preference of WT-CALB for the (*R*)-*sec* alcohols moiety probably plays a role. For the stereodivergent mutants, distinct trends were observed. For example, compared to WT CALB, the  $k_{\text{cat}}/K_m$  of Mutant-*R*<sub>acid</sub>*S*<sub>alco</sub> for (2*R*, 1'*R*)-**3a** and (2*S*, 1'*R*)-**3a** decreased from 428 and 674 to 2.7 and 0.3 M<sup>-1</sup>s<sup>-1</sup>, respectively, while the  $k_{\text{cat}}/K_m$  for (2*R*, 1'*S*)-**3a** increased from essentially 0 to 155 M<sup>-1</sup>s<sup>-1</sup>. Similarly, Mutant-*S*<sub>acid</sub>*S*<sub>alco</sub> displays high  $k_{\text{cat}}/K_m$  (339 M<sup>-1</sup>s<sup>-1</sup>) for (2*S*, 1'*R*)-**3a**, while it hardly transforms other enantiomers. In the case of Mutant-*R*<sub>acid</sub>*R*<sub>alco</sub> and *S*<sub>acid</sub>*R*<sub>alco</sub>, the preference of the respective (2*R*, 1'*R*)- and (2*S*, 1'*R*)-enantiomers is also clearly indicated by the correspondingly increased  $k_{\text{cat}}/K_m$  (Table 2).

**Crystallography.** To better understand the relationship between the manipulated stereoselectivities and specific protein structures, we obtained X-ray crystal structures of the four best mutants at 1.60–1.83-Å resolution (Table S7). Each mutant contains two chains in one asymmetric unit, and the two monomers have almost the same structure of the protein scaffold, except for loop 140–147, which displays open and closed conformations, respectively (Fig. 3 and Fig. S1). Different from that found by Stauch et al. (PDB: 5A71),<sup>30</sup> our closed conformation is similar to the structure reported by Uppenberg et al. (PDB: 1TCA).<sup>20b</sup> In the open chain conformation, the flexible loop 140–147 is located away from the entrance of the reaction chamber relative to WT CALB, thereby exposing the active site. Our B-factor analysis<sup>31</sup> of loop 140–147 in all four mutants indicates higher flexibility relative to that in CALB-WT (PDB: 1TCA).<sup>20b</sup> The structural promiscuity of the variants around the substrate entrance may account for their lower  $K_m$  values compared to that of WT, especially toward the preferred stereoisomers. Remarkably, the four stereodivergent variants display significantly different structures of the respective active sites (Fig. 3B–E). Variants with the same selectivity toward the acid moiety show a similar shape of the acid pocket, for example Mutant-*R*<sub>acid</sub>*R*<sub>alco</sub> vs. Mutant-*R*<sub>acid</sub>*S*<sub>alco</sub>, or Mutant-*S*<sub>acid</sub>*R*<sub>alco</sub> vs. Mutant-*S*<sub>acid</sub>*S*<sub>alco</sub>. The (*R*)-acid selectivity pockets of Mutant-*R*<sub>acid</sub>*R*<sub>alco</sub> and *R*<sub>acid</sub>*S*<sub>alco</sub> have the same V190 residue and relatively small 189 residue (A and V), while the (*S*)-acid selectivity pockets of Mutant-*S*<sub>acid</sub>*R*<sub>alco</sub> and *S*<sub>acid</sub>*S*<sub>alco</sub> have the same C190 residue and a relatively large 189 residue (I and M). Similarly, (*R*)-alcohol-selective Mutants-*R*<sub>acid</sub>*R*<sub>alco</sub> and *S*<sub>acid</sub>*R*<sub>alco</sub> have a small space of the alcohol-binding pockets due to large W104 position, while Mutants-*R*<sub>acid</sub>*S*<sub>alco</sub> and *S*<sub>acid</sub>*S*<sub>alco</sub> have large and deep alcohol-binding pockets with a preference for (*S*)-alcohols.

Further, we attempted to get a complex structure which shows how the substrates or products dock in the reaction

pocket. Since **3a** and **1a** are easily hydrolyzed by CALB mutants under most crystallization conditions, 1-phenethylamine 2-phenyl propionic (**3a'**) was used as an analog. Unfortunately, only one complex of Mutant-*S*<sub>acid</sub>*R*<sub>alco</sub> with (2*S*, 1'*R*)-**3a'** at the reaction site crystallized for X-ray analysis (Fig. S2). As in the case of the apo-protein, two monomers make up an asymmetric unit in the complexed structure. Substrate (2*S*, 1'*R*)-**3a'** was found to be located slightly next to the catalytic site of the open monomer, with an occupancy of 91%. As expected, the methyl-group of the alcohol moiety points to the alcohol-binding pocket, surrounded by W104, while the phenyl is kept out of the entrance. Unfortunately, it was not possible to identify the exact binding mode of the acid part.

**Unveiling the Source of Differing Stereoselectivity of CALB Variants.** To obtain some insight regarding the source of differing stereoselectivity of the four highly stereocomplementary CALB variants, four enantiomeric ligands of **3a** were docked into the binding pockets of variants *R*<sub>acid</sub>*R*<sub>alco</sub>, *S*<sub>acid</sub>*R*<sub>alco</sub>, *R*<sub>acid</sub>*S*<sub>alco</sub> and *S*<sub>acid</sub>*S*<sub>alco</sub>, respectively, and 100-ns molecular dynamic (MD) simulations were conducted. For the MD simulated structure, we measured in particular the distance between the S105 oxygen of the catalytic triad and the carbonyl carbon of the ester substrate (Fig. S3). In all four cases, the shortest distance proved to be the one that leads to the observed stereoselectivity. The binding enthalpies of the four ester enantiomers in the variants were calculated using the MM/GBSA method.<sup>32</sup> It can be seen that the order of binding enthalpies correlates with the respective stereoselectivities: The stronger, the more selective (Table S8). Since the entropy changes would be similar when the four different stereoisomeric ligands bind with a same variant, only the enthalpies were computed and the entropy contributions were neglected in these calculations (Eq. 2 in supporting information).

The MD results also show that the binding modes of the four stereoisomers in their respective stereoselective variants are divergent. From the MD structure comparison between the complex of Mutant-*R*<sub>acid</sub>*R*<sub>alco</sub> (I189A/Q157L) and (2*R*, 1'*R*)-**3a**, and the complex of Mutant-*S*<sub>acid</sub>*R*<sub>alco</sub> (V190C/A281G/A282V) and (2*S*, 1'*R*)-**3a** (Fig. 4A, C & D), it was found that the binding modes of the two enantiomers in their corresponding optimal mutants are completely different, which are relevant to their different enantioselectivity. In the Mutant-*R*<sub>acid</sub>*R*<sub>alco</sub> complex, the methyl substituent of the acid moiety of (2*R*, 1'*R*)-**3a** points to L157 position, while the hydrogen atom pointing to I189 at the loop 184–194 (Fig. 4A, D). In Mutant-*S*<sub>acid</sub>*R*<sub>alco</sub>, the orientation of methyl and hydrogen of (2*S*, 1'*R*)-**3a** is reversed (Fig. 4A, C). The benzene group of the acid moiety in both enantiomers have the similar orientation, pointing to the entrance of the acid pocket. Moreover, the whole pocket of Mutant-*S*<sub>acid</sub>*R*<sub>alco</sub> for binding alcohol and acid is more closed than that of Mutant-*R*<sub>acid</sub>*R*<sub>alco</sub> (I189A/Q157L) (Fig. 4A), due to the different movement of

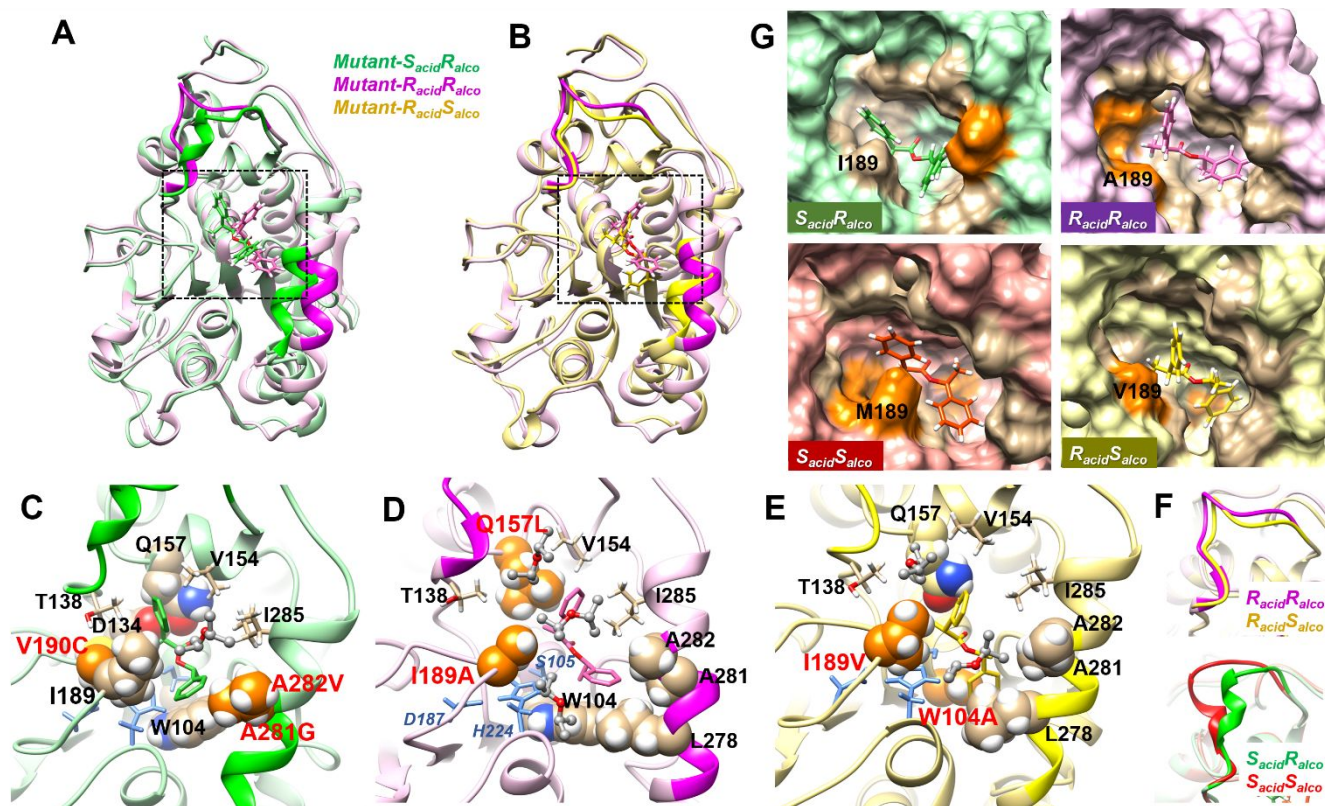


**Figure 4.** MD-simulated binding modes of various enantiomers in their respective selective CALB variants. (A) Cartoon representation comparison of (2S, 1'R)-3a enantiomer bound in Mutant-*S*<sub>acid</sub>*R*<sub>alco</sub> (green) and (2R, 1'R)-3a enantiomer in Mutant-*R*<sub>acid</sub>*R*<sub>alco</sub> (purple). (B) Cartoon representation comparison of (2R, 1'R)-3a enantiomer in Mutant-*R*<sub>acid</sub>*R*<sub>alco</sub> (purple) and (2R, 1'S)-3a enantiomer in Mutant-*R*<sub>acid</sub>*S*<sub>alco</sub> (yellow). C-E images are the enlarged binding modes of (2S, 1'R)-3a enantiomer in Mutant-*S*<sub>acid</sub>*R*<sub>alco</sub> (C), (2R, 1'R)-3a enantiomer in Mutant-*R*<sub>acid</sub>*R*<sub>alco</sub> (D) and (2R, 1'S)-3a enantiomer in Mutant-*R*<sub>acid</sub>*S*<sub>alco</sub> (E). (F) Structure comparison of the lid 140-149 of four different mutants. (G) The surface of the binding pocket of four different mutants binding with their respective enantiomers. In images C-E, the mutated residues are represented by orange sphere, and other representative residues are represented by sphere or sticks with different color. The catalytic triad (S105-H224-D187) in C-E are colored in light blue. In image G, the mutated residues are represented by orange surface.

the lid 140-149 and the helix 265-285 caused by corresponding mutations.

In the case of (2R, 1'R)-3a binding in the Mutant-*R*<sub>acid</sub>*R*<sub>alco</sub> (I189A/Q157L), the ligand is exposed to three IPE solvent molecules (Fig. 4D). Compared the apo variant, the binding of the ligand pushes the 265-285 helix away from the active site and I285 moves closer to the benzene group of the acid moiety (Fig. S6B). Accordingly, L278 moves away from the alcohol moiety and L277 becomes fully exposed pointing outward the binding site. As a result, a large entrance to the alcohol pocket is formed to accommodate the benzene-moiety of the alcohol moiety (Fig. 4D, 4G and S6B) and the methyl group of the alcohol portion forms favorable hydrophobic interaction with W104, which accounts for the high selectivity toward the (*R*)-secondary alcohol part. The phenyl group of the alcohol moiety is nested in a hydrophobic domain formed by H224, L278, A282 and I285 (Fig. 4D). On the other hand, with the ligand bound, the lid region exhibits a more open conformation compared to the Mutant-*S*<sub>acid</sub>*R*<sub>alco</sub> complex. The incorporation of medium size leucine at position 157 provides suitable space and hydrophobic interaction with the methyl of the acid moiety, such that smaller or larger mutations caused the decrease of target selectivity (Fig.2B). The pointing of methyl to L157 pushes the ligand closer the helix 265-285.

Meanwhile, the mutation of I189A provides a relative large space to accommodate the chiral center containing a large benzene group of the acid moiety. The benzene of the acid moiety forms hydrophobic interactions with V154, L157, I285 and A189 (Figs. 4D).

With the ligand (2S, 1'R)-3a binding, the phenyl group of the alcohol moiety establishes favorable hydrophobic interactions with H224, L278 and V282 in Mutant-*S*<sub>acid</sub>*R*<sub>alco</sub> (V190C/A281G/A282V) (Fig. 4C, S5A and S6A). The conformational change around the helix 265-285 induced by A282V/A281G mutations results in a closed alcohol pocket (Fig. 4A, 4C and 4G). The methyl group of the alcohol portion forms favorable hydrophobic interaction with W104 and thereby accounts for the high selectivity toward the (*R*)-secondary alcohol part. On the other hand, the V190C mutation causes the conformational change of the loop where it is located. As a result, the acid-selective pocket of CALB is reshaped and the orientation of methyl and hydrogen of (2S, 1'R)-3a is reversed compared with the complex of Mutant-*R*<sub>acid</sub>*R*<sub>alco</sub> accounting for the (*S*)-selectivity of the acid pocket. The benzene of acid moiety forms hydrophobic interactions with I189, as well as T138, Q157 and V154.

Similar differences between the orientation of the acid moiety in (2R, 1'S)-3a and (2S, 1'S)-3a enantiomers in their



optimal mutants are also observed (Fig. S4B and 4G). Interestingly, two mutants with the same acid-selectivity show the similar conformation of the lid 140-149 (Fig. 4F).

Additionally, the MD structure comparison between the complex of Mutant- $R_{\text{acid}}R_{\text{alco}}$  (I189A/Q157L) and (2*R*, 1'*S*)-**3a**, and the complex of Mutant- $R_{\text{acid}}S_{\text{alco}}$  (W104A/I189V) and (2*R*, 1'*S*)-**3a** (Fig 4B) offers insight about the source of different *sec*-alcohol stereoselectivity of CALB variants. It was found that both the conformation of the acid pockets of the two mutants and the orientation of their ligands are very similar, implying their similar acid-selectivity. The reversion of alcohol selectivity was mainly caused by the W104A mutation, which creates extra space for the accommodation of large-sized benzene group in the alcohol moiety of ligands, and therefore accounts for the reversed (*S*)-alcohol-selectivity for (2*R*, 1'*S*)-**3a** in Mutant- $R_{\text{acid}}S_{\text{alco}}$  (W104A/I189V) (Fig. 4E and 4G). W104A mutation not only changes the alcohol selectivity, but also influences the binding mode of the acid moiety of the ligand. The whole ligand moves closer to the helix 265-285, due to the sliding of the benzene of the alcohol moiety into the alcohol-binding pocket (Fig. 4B and 4E). This movement provides extra space for the methyl substituent pointing to Q157, accounting for the astonishing increase of (*R*)-acid selectivity from essentially 0 (WT) to 81% (W104A) (Fig. 2C). Moreover the mutation of I189V further improves this selectivity, similar to that in the case of Mutant- $R_{\text{acid}}R_{\text{alco}}$  (Fig. 4G and 2C).

**Conclusions and Perspectives.** In summary, by way of a highly focused protein engineering method dubbed “focused rational iterative site-specific mutagenesis” (FRISM), we have addressed the challenging issue of stereodivergent engineering of *Candida antarctica* lipase (CALB) with generation of four highly stereocomplementary variants needed to access catalytically all four stereoisomers bearing two stereocenters in transesterification reactions between racemic acids and racemic alcohols in an organic solvent. Although non-aqueous reaction conditions are known to be challenging in directed enzyme evolution,<sup>16,24a</sup> our FRISM strategy required the generation and screening of less than a total of 100 transformants in the quest to achieve >90% selectivity for all of the four possible stereoisomers in the model reaction. This was accomplished by first applying exploratory site-directed mutagenesis at 7 selected sites lining the binding pocket of CALB using only 3 representative amino acids, including alanine (A), leucine (L), and phenylalanine (F). Following the identification of key mutations at the identified hotspots, further site-specific mutagenesis was performed iteratively using similar-sized amino acids (A<sup>+</sup>: G; L<sup>+</sup>: V/C/I/M; F<sup>+</sup>: Y/W). Saturation mutagenesis with formation of traditional libraries was not needed.

In most previous protein engineering studies of CALB or other lipases, the respective binding pocket was “divided” into two parts, the acid (acyl) and the alcohol binding domains.<sup>21,22</sup> Mutations were then restricted to the chirality-containing domain, defined by the nature of the substrate. In the present study, however, we discovered that mutations in one domain influence the stereoselectivity of the other, a result of “remote” effects.

The experimental results concerning complete control of both absolute and relative configuration in compounds having two stereogenic centers, catalyzed by CALB mutants, are of synthetic significance because they provide access to all

possible stereoisomers, as in the case of the therapeutic drug candidates of the ibuprofen-type (Table 1). Moreover, both chiral alcohols and acids are extensively used in pharmaceutical industry, and the four stereodivergent enantiomers can be hydrolyzed to obtain optical pure acids and alcohols, simultaneously. The best stereocomplementary mutants display relatively broad substrate scopes, except for Mutant- $S_{\text{acid}}S_{\text{alco}}$ . Importantly, a significant tradeoff in thermostability was not observed in the evolved variants. Consequently, the range of CALB applications has been expanded considerably. In order to gain structural insight into the source of stereodivergent selectivity of the four best mutants, crystals were grown and studied by X-ray analysis, flanked by docking studies and molecular dynamics (MD) simulations.

Finally, we point out that the FRISM method of protein engineering constitutes a logical fusion of rational design<sup>21,24,33</sup> and directed evolution.<sup>14,16</sup> The decisions concerning the choice of the amino acids in the site-specific mutagenesis steps can be supported by X-ray structural and consensus data as well as computational aids such as machine learning<sup>34</sup> or Rosetta design.<sup>33d</sup> We expect that in the future, FRISM will be used in the protein engineering studies of other enzymes for enhancing stereo- and regioselectivity as well as activity and/or thermostability.

## MATERIALS AND METHODS

**Library Generation.** The PCR (50  $\mu$ L final volume) contained: ddH<sub>2</sub>O (29  $\mu$ L), Pfu 10X buffer (5  $\mu$ L), dNTP (4  $\mu$ L, 2.5 mM each), forward primers (5  $\mu$ L, 2.5  $\mu$ M each), silent reverse primer (GATGCCGGGAGCAGACAAGCCCCGTACGGGCGC, 5  $\mu$ L, 2.5  $\mu$ M), template plasmid (pETM11-CALB, 1.0  $\mu$ L, 100 ng/ $\mu$ L) and 1  $\mu$ L of Pfu polymerase. PCR conditions used were 94  $^{\circ}$ C, 5 min; 30 cycles of (94  $^{\circ}$ C, 1 min; 60  $^{\circ}$ C, 1 min; 72  $^{\circ}$ C, 14 min) and final extension at 72  $^{\circ}$ C, 10 min. Then, the PCR mixtures were mixed with 2  $\mu$ L DpnI (10 U/ $\mu$ L) and incubated overnight at 37  $^{\circ}$ C. The product was purified with an Omega PCR purification spin column, and an aliquot of 15  $\mu$ L was used to transform 80  $\mu$ L of electrocompetent *E. coli* BL21 (DE3) cells, which contain chaperone plasmid pGro7 (Takara, Japan). The transformation mixture was incubated with 1 mL of LB medium at 37  $^{\circ}$ C under shaking of 200 rpm for 1 hour and spread on LB-agar plates containing Kanamycin (34 mg/L) and Chloramphenicol (34 mg/L), and the plates were incubated for 16-24 hours. A single colony was picked and incubated in 5 mL of LB medium at 37  $^{\circ}$ C overnight. The plasmid was extracted with an Omega gel extraction column, and sequenced by Sangon Biotech (Shanghai, China). Target mutants were stored with glycerol at -80  $^{\circ}$ C.

**Scaffold Expression.** 100  $\mu$ L stored bacteria were first inoculated in 5ml LB medium (containing 34  $\mu$ g/mL Kanamycin and 34  $\mu$ g/mL Chloramphenicol), and shaken overnight as preculture. A fresh 1L of TB medium with 1.0 mg/mL L-arabinose as the inducer for expression of chaperone pGro7 and the same concentration antibiotics as above, was inoculated from 5 mL preculture. The cultures were allowed to grow at 37  $^{\circ}$ C until OD (600) at 0.6~0.8. After cooling at 4 $^{\circ}$ C for 1h, 1.0 mM isopropyl  $\beta$ -thiogalactopyranoside (IPTG) was added to induce CALB expression. The cultures were allowed to express at 16  $^{\circ}$ C for 48h with shaking at 200 rpm. Then

cells were harvested by centrifugation at 9000 rpm and 4 °C for 10 min and the supernatants were discarded. The cells were resuspended in 20 mL 50 mM phosphate buffer (pH 7.4) and stored at -80 °C.

**Purification and Immobilization of CALB Mutants.** The cells were subjected to repeated freezing and thawing for 3 times, and then the target proteins were released by sonication. The cell debris was removed by centrifugation at 12,000 rpm for 15 min at 4.0 °C. The supernatant was filtered and loaded on a GE Healthcare HisTrap FF Crude column (5 mL) pre-equilibrated with 50 mM phosphate buffer (pH 7.4) containing 0.5 M NaCl and 5 mM imidazol. Impurity and chaperone were removed by imidazol at the concentration of about 70 mM and the enzyme was eluted by 50 mM Tris-HCl buffer with 0.5 M NaCl and 200 mM imidazol. The proteins were dialyzed by 50 mM phosphate buffer (pH 7.4) for one day at 4 °C. Then, the purified enzyme solution was mixed with acrylic resin in 50 mL EP tube and stirred end-over-end rotation at 20 °C, overnight. Then, the resin was filtered and freeze-dried in vacuo. The immobilized lipase was used for the kinetic resolution in organic phase.

**General Procedure for Kinetic Resolution of Substrates.** 50 mg immobilized CALB (10% enzyme on acrylic resin) was added to 1 mL anhydrous IPE containing substrates *rac*-**1a** (50mM) and *rac*-**2a** (45mM), and this mixture was shaken at 200 rpm and 37 °C for about 12 h. The reaction mixture was filtered and evaporated in vacuo. Conversion and selectivity were determined by chiral HPLC using specific conditions as shown in the section of HPLC chromatograms. The crude products were purified by silica gel chromatography (petroleum ether and ethyl acetate).

**Scale-up of Kinetic Resolution of Substrate (2*S*, 1'*R*)-**3a** and (2*S*, 1'*R*)-**3r**.** 150 mg immobilized CALB (10% enzyme on acrylic resin) was added to 5 mL anhydrous IPE containing **1a** (or **1r**) (500mM) and **2a** (450mM), and this mixture was shaken at 200 rpm and 37 °C for about 48h. The process was monitored by chiral HPLC. The mixture was filtered and evaporated under reduced pressure, and purified by column chromatography to provide the corresponding (2*S*, 1'*R*)-**3a** with 37% isolated yield (211 mg), 96/4 d.r. and 99/1 e.r., and (2*S*, 1'*R*)-**3r** with 40% isolated yield (279 mg), 93/7 d.r. and 99/1 e.r., respectively.

**X-ray Structure Determination.** Four best variants, Mutant-*R*<sub>acid</sub>*R*<sub>alco</sub>, Mutant-*S*<sub>acid</sub>*R*<sub>alco</sub>, Mutant-*S*<sub>acid</sub>*S*<sub>alco</sub>, Mutant-*R*<sub>acid</sub>*S*<sub>alco</sub> and Mutant-*S*<sub>acid</sub>*R*<sub>alco</sub> in complex with **3a'** were crystallized by using the sitting-drop vapor diffusion method at 18 °C. All crystals were mounted in nylon loops and flash-frozen in liquid nitrogen. All diffraction data was collected at the wavelength of 0.97775 Å on SSRF beamline 19U1 of the National Center for Protein Science Shanghai (China). All data collection was performed at 100 K. All data sets were indexed, integrated, and scaled using the HKL2000 package.<sup>35</sup> The apo-mutant structures were solved by molecular replacement method using the program PHASER,<sup>36</sup> and the structure of WT-CALB (PDB code 1TCA) as a search model. The complex structure was solved by the same method using the structure of Mutant-*S*<sub>acid</sub>*R*<sub>alco</sub> as a search model. Rounds of automated refinement were performed with PHENIX,<sup>37</sup> and the models were extended and rebuilt manually with COOT.<sup>38</sup> The statistics for data collection and crystallographic refinement are summarized in supporting information. The atomic coordinates of four best variants Mutant-*R*<sub>acid</sub>*R*<sub>alco</sub>

(PDB Code 6J1R), Mutant-*R*<sub>acid</sub>*S*<sub>alco</sub> (PDB Code 6J1Q), Mutant-*S*<sub>acid</sub>*R*<sub>alco</sub> (PDB Code 6J1P), and Mutant-*S*<sub>acid</sub>*S*<sub>alco</sub> (PDB Code 6J1S), and Mutant-*S*<sub>acid</sub>*R*<sub>alco</sub> in complex with **3a'** (PDB Code 6J1T) have been deposited in the Protein Data Bank (PDB).

## ASSOCIATED CONTENT

### Supporting Information.

This material is available free of charge via the Internet at <http://pubs.acs.org>. Complete experimental procedures, details of molecular calculations, all chiral chromatograms and NMR spectra of products.

## AUTHOR INFORMATION

### Corresponding Author

\*wuqi1000@163.com, or llc123@zju.edu.cn;

\*reetz@mpi-muelheim.mpg.de;

\*m.huang@qub.ac.uk;

\*jiahai@mail.sioc.ac.cn;

### ORCID

Qi Wu: 0000-0001-9386-8068

Manfred T. Reetz: 0000-0001-6819-6116

### Author Contributions

‡These authors contributed equally.

### Notes

The authors declare no competing financial interest.

## ACKNOWLEDGMENT

Q.W. and X.F.L. thank the National Natural Science Foundation of China (21574113, 21472169), Natural Science Foundation of Zhejiang Province (LY19B020014), and the Fundamental Research Funds for the Central Universities (2018QNA3010) for funding support. M.H. thanks INVEST NI Research and Development Programme for funding support. J.Z. thanks the Strategic Priority Research Program (B) of the Chinese Academy of Sciences (XDB20000000) for funding support. M.T.R. thanks the Max-Planck-Society and the Arthur C. Cope Fund for financial support. We thank the staffs from BL19U1 at Shanghai Synchrotron Radiation Facility (SSRF, China) for assistance during X-ray data collection.

## REFERENCES

- (1) (a) *Drug Stereochemistry: Analytical Methods and Pharmacology*, 3<sup>rd</sup> ed.; Jóźwiak, K., Lough, W. J., Wainer, I. W., Eds.; CRC Press: Boca Raton, FL, 2012. (b) *The Practice of Medicinal Chemistry*, 3<sup>rd</sup> ed.; Wermuth, C. G., Ed.; Elsevier: Amsterdam, 2008.
- (2) Bren, L. Frances Oldham Kelsey. FDA Medical Reviewer Leaves Her Mark on History. *FDA Consum.* **2001**, 35(2), 24-29.
- (3) (a) Zhang, A. P.; Xie, X. M.; Liu, W. P. Enantioselective Separation and Phytotoxicity on Rice Seedlings of Paclobutrazol. *J. Agri Food Chem* **2011**, 59, 4300-4305.
- (4) (a) Wilkinson, R. G.; Shepherd, R. G.; Thomas, J. P.; Baughn, C. Stereospecificity in a New Type of Synthetic Antituberculous Agent. *J. Am. Chem. Soc.* **1961**, 83, 2212-2213. (b) Rubin-Preminger, J. M.; Bernstein, J.; Harris, R. K.; Evans, I. R.; Ghi, P. Y. Variable Temperature Studies of a Polymorphic System Comprising Two Pairs of Enantiotropically Related Forms: [S,S]-Ethinbutol Dihydrochloride. *Cryst. Growth Des.* **2004**, 4(3), 431-439.



(5) (a) Gridnev, I. D.; P. A. Dub, *Enantioselection in Asymmetric Catalysis*, CRC Press, 2016. (b) Blaser, H.-U.; Schmidt, E. (eds), *Asymmetric Catalysis on Industrial Scale: Challenges, Approaches and Solutions*, Wiley-VCH, Weinheim, 2011. (c) Walsh, P. J.; Kozlowsky, M. C., *Fundamentals of Asymmetric Catalysis*, University Science Books, 2009.

(6) E. N. Jacobsen. Asymmetric catalysis of epoxide ring-opening reactions, *Acc. Chem. Res.* **2000**, *33*, 421-431.

(7) (a) Krautwald, S.; Sarlah, D.; Schafroth, M. A.; Carreira, E. M. Enantio- and Diastereodivergent Dual Catalysis:  $\alpha$ -Allylation of Branched Aldehydes, *Science* **2013**, *340*, 1065-1068. (b) Sandmeier, T.; Krautwald, S.; Zipfel, H.F.; Carreira, E.M. Stereodivergent Dual Catalytic  $\alpha$ -Allylation of Protected  $\alpha$ -Amino- and  $\alpha$ -Hydroxyacetaldehydes, *Angew. Chem. Int. Ed.* **2015**, *54*, 14363 – 14367.

(8) Shi, S.-L.; Wong, Z. L.; Buchwald, S. L. Copper-catalysed Enantioselective Stereodivergent Synthesis of Amino Alcohols, *Nature* **2016**, *532*, 353-356.

(9) Selected reviews of catalysis involving more than one stereocenter: (a) Krautwald, S.; Carreira, E. M. Stereodivergence in Asymmetric Catalysis, *J. Am. Chem. Soc.* **2017**, *139*, 5627–5639; (b) Bihani, M.; Zhao, J.C.G. Advances in Asymmetric Diastereodivergent Catalysis, *Adv. Synth. Catal.* **2017**, *359*(4), 534-575. (c) Bhat, V.; Welin, E.R.; Guo, X.L.; Stoltz, B. M. Advances in Stereoconvergent Catalysis from 2005 to 2015: Transition-Metal-Mediated Stereoablative Reactions, Dynamic Kinetic Resolutions, and Dynamic Kinetic Asymmetric Transformations, *Chem. Rev.* **2017**, *117*(5), 4528–4561. (d) Zheng, C.; You, S.L. Catalytic Asymmetric Dearomatization by Transition-Metal Catalysis: A Method for Transformations of Aromatic Compounds, *Chem* **2016**, *1*, 830–857. (e) Trost, B.M.; Rao, M. Development of Chiral Sulfoxide Ligands for Asymmetric Catalysis, *Angew. Chem. Int. Ed.* **2015**, *54*, 5026–5043. (f) Chen, D.F.; Han, Z.Y.; Zhou, X.L.; Gong, L.Z. Asymmetric Organocatalysis Combined with Metal Catalysis: Concept, Proof of Concept, and Beyond, *Acc. Chem. Res.* **2014**, *47*, 2365–2377. (g) Brak, K.; Jacobsen, E.N. Asymmetric Ion-Pairing Catalysis, *Angew. Chem. Int. Ed.* **2013**, *52*, 534-561. (h) Mahlau, M.; List, B. Asymmetric Counteranion-Directed Catalysis: Concept, Definition, and Applications, *Angew. Chem. Int. Ed.* **2013**, *52*, 518-533. (i) Yoon, M.; Srirambalaji, R.; Kim, K. Homochiral Metal–Organic Frameworks for Asymmetric Heterogeneous Catalysis, *Chem. Rev.* **2012**, *112*, 1196–1231. (j) Shibasaki, M.; Kanai, M.; Matsunaga, S.; Kumagai, N. Recent Progress in Asymmetric Bifunctional Catalysis Using Multimetallic Systems, *Acc. Chem. Res.* **2009**, *42*, 1117–1127.

(10) Reviews of enzyme catalysis in organic and pharmaceutical chemistry: (a) *Biocatalysis in the Pharmaceutical and Biotechnology Industries*, Patel, R. N. (ed.), CRC Press, 2006. (b) Goswami, A.; Stewart, J. D., *Organic Synthesis Using Biocatalysts*, Academic Press, 2015. (c) *Enzyme Catalysis in Organic Synthesis*, Drauz, K., Gröger, H., May, O. (eds.), Wiley-VCH, Weinheim, 2012. (d) Faber, K., *Biotransformations in Organic Chemistry: A Textbook*, Springer, Stuttgart, 2011. (e) Liese, A.; Seelbach, K.; Wandrey, C., *Industrial Biotransformations*, Wiley-VCH, Weinheim, 2006.

(11) Archelas, A.; Iacazio, G.; Kotik, M. Epoxide hydrolases and their application in organic synthesis, in *Green Biocatalysis* (Patel, R. N., ed.), Wiley, 2016: 978-1-118-82229-6.

(12) Li, A.; Ilie, A.; Sun, Z.; Lonsdale, R.; Xu, J.H.; Reetz, M.T. Whole-Cell-Catalyzed Multiple Regio- and Stereoselective Functionalizations in Cascade Reactions Enabled by Directed Evolution, *Angew. Chem. Int. Ed.* **2016**, *55*, 12026-12029.

(13) Erdmann, V.; Lichman, B.R.; Zhao, J.; Simon, R. C.; Kroutil, W.; Ward, J.M.; Hailes, H.C.; Rother, D. Enzymatic and Chemoenzymatic Three-Step Cascades for the Synthesis of Stereochemically Complementary Trisubstituted Tetrahydroisoquinolines, *Angew. Chem. Int. Ed.* **2017**, *56*, 12503-12507.

(14) Reetz, M. T. Laboratory Evolution of Stereoselective Enzymes: A Prolific Source of Catalysts for Asymmetric Reactions, *Angew. Chem. Int. Ed.* **2011**, *50*, 138-174.

(15) Mugford, P. F.; Wagner, U. G.; Jiang, Y.; Faber, K.; Kazlauskas, R. J. Enantiocomplementary Enzymes: Classification,

Molecular Basis for Their Enantioference, and Prospects for Mirror-image Biotransformations. *Angew. Chem., Int. Ed.* **2008**, *47*, 8782–8793.

(16) For selected reviews of directed evolution,<sup>14</sup> see: (a) Turner, N. J. Directed Evolution Drives the Next Generation of Biocatalysts, *Nat. Chem. Biol.* **2009**, *5*, 567–573. (b) Currin, A.; Swainston, N.; Day, P. J.; Kell, D. B. Synthetic Biology for the Directed Evolution of Protein Biocatalysts: Navigating Sequence Space Intelligently, *Chem. Soc. Rev.* **2015**, *44*, 1172–1239. (c) Denard, C. A.; Ren, H.; Zhao, H. Improving and Repurposing Biocatalysts via Directed Evolution, *Curr. Opin. Chem. Biol.* **2015**, *25*, 55–64. (d) Reetz, M. T. Directed Evolution of Selective Enzymes: Catalysts for Organic Chemistry and Biotechnology, Wiley-VCH Weinheim, (2016). (e) Hammer, S. C.; Knight, A. M.; Arnold, F. H. Design and Evolution of Enzymes for Non-natural Chemistry, *Curr. Opin. Green Sustain. Chem.* **2017**, *7*, 23-30. (f) Zeymer, C.; Hilvert, D. Directed Evolution of Protein Catalysts, *Annu. Rev. Biochem.* **2018**, *87*, 131-157.

(17) Roiban, G.-D.; Agudo, R.; Reetz, M. T. Cytochrome P450 Catalyzed Oxidative Hydroxylation of Achiral Organic compounds with Simultaneous Creation of Two Chirality Centers in a Single C-H Activation Step, *Angew. Chem. Int. Ed.* **2014**, *126*, 8803-8807.

(18) (a) Knight, A.M.; Jennifer Kan, S. B.; Lewis, R.D.; Brandenberg, O. F.; Chen, K.; Arnold, F.H. Diverse Engineered Heme Proteins Enable Stereodivergent Cyclopropanation of Unactivated Alkenes, *ACS Cent. Sci.*, **2018**, *4*, 372–377. (b) Bajaj, P.; Sreenilayam, G.; Tyagi, V.; Fasan, R. Gram-Scale Synthesis of Chiral Cyclopropane-Containing Drugs and Drug Precursors with Engineered Myoglobin Catalysts Featuring Complementary Stereoselectivity, *Angew. Chem., Int. Ed.* **2016**, *55*, 16110–16114. (c) Tinoco, A.; Steck, V.; Tyagi, V.; Fasan, R. Highly Diastereo- and Enantioselective Synthesis of Trifluoromethyl Substituted Cyclopropanes via Myoglobin-Catalyzed Transfer of Trifluoromethylcarbene, *J. Am. Chem. Soc.* **2017**, *139*, 5293–5296

(19) Garrabou, X.; Macdonald, D. S.; Wicky, B.I.M.; Hilvert, D. Stereodivergent Evolution of Artificial Enzymes for the Michael Reaction, *Angew. Chem. Int. Ed.* **2018**, *57*, 5288–5291

(20) Selected key studies and reviews of CALB: (a) Anderson, E. M.; Larsson, K. M.; Kirk, O. One Biocatalyst-many Applications: the Use of *Candida Antarctica* B-lipase in Organic Synthesis, *Biocatal.* **1998**, *16*, 181 – 204. (b) Uppenberg, J.; Hansen, M. T.; Patkar, S.; Jones, T. A. The Sequence, Crystal Structure Determination and Refinement of Two Crystal Forms of Lipase B from *Candida Antarctica*, *Structure* **1994**, *2*, 293-308. (c) Otto, R. T.; Scheib, H.; Bornscheuer, U. T.; Pleiss, J.; Syltatk, C.; Schmid, R. D. Substrate Specificity of Lipase B from *Candida Antarctica* in the Synthesis of Arylaliphatic Glycolipids, *J. Mol. Catal. B: Enzym.* **2000**, *8*, 201–211.

(21) Key studies of protein engineering of CALB using rational design: (a) Magnusson, A. O.; Takwa, M.; Hamberg, A.; Hult, K. An S-selective Lipase was Created by Rational Redesign and the Enantioselectivity Increased with Temperature, *Angew. Chem. Int. Ed.* **2005**, *117*, 4658-4661. (b) Engström, K.; Vallin, M.; Syrén, P. O.; Hult, K.; Bäckvall, J. E. Mutated Variant of *Candida Antarctica* Lipase B in (S)-selective Dynamic Kinetic Resolution of Secondary Alcohols, *Org. Biomol. Chem.* **2011**, *9*, 81–82. (c) Marton, Z.; Léonard-Nevers, V.; Syrén, P.-O.; Bauer, C.; Lamare, S.; Hult, K.; Tranc, V.; Graber, M. Mutations in the Stereospecificity Pocket and at the Entrance of the Active Site of *Candida Antarctica* Lipase B Enhancing Enantioselectivity, *J. Mol. Catal. B: Enzym.* **2010**, *65*, 11–17. (d) Larsen, M. W.; Zielinska, D. F.; Martinelle, M.; Hidalgo, A.; Juhl Jensen, L.; Bornscheuer, U. T.; Hult, K. Suppression of Water as a Nucleophile in *Candida Antarctica* Lipase B Catalysis, *ChemBioChem*, **2010**, *11*, 796–801.

(22) Selected studies of protein engineering of CALB using directed evolution<sup>21</sup>: (a) Qian, Z.; Fields, C. J.; Lutz, S. Investigating the Structural and Functional Consequences of Circular Permutation on Lipase B from *Candida Antarctica*, *ChemBioChem* **2007**, *8*, 1989–1996. (b) Qin, B.; Liang, P.; Jia, X.; Zhang, X.; Mu, M.; Wang, X.Y.; Ma, G.Z.; Jin, D.N.; You, S. Directed Evolution of *Candida Antarctica* Lipase B for Kinetic Resolution of Profen Esters, *Catal. Commun.* **2013**, *38*, 1–5. (c) Wu, Q.; Soni, P.; Reetz, M.T. Laboratory

Evolution of Enantiocomplementary *Candida Antarctica* Lipase B Mutants with Broad Substrate Scope. *J. Am. Chem. Soc.* **2013**, *135*, 1872–1881.

(23) (a) Steinreiber, J.; Faber, K.; Griengl, H. De-racemization of Enantiomers versus De-epimerization of Diastereomers - Classification of Dynamic Kinetic Asymmetric Transformations (DYKAT). *Chem. Eur. J.* **2008**, *14*, 8060–8072. (b) Schober, M.; Faber, K. Inverting Hydrolases and Their Use in Enantioconvergent Biotransformations. *Trends Biotechnol.* **2013**, *31*, 468–478.

(24) (a) Wikmark, Y.; Svedendahl Humble, M.; Bäckvall, J.-E. Combinatorial Library Based Engineering of *Candida Antarctica* Lipase A for Enantioselective Transacylation of Sec-alcohols in Organic Solvent. *Angew. Chem. Int. Ed.* **2015**, *54*, 4284–4288. (b) Sandström, A.G.; Wikmark, Y.; Engström, K.; Nyhlén, J.; Bäckvall, J.-E. Combinatorial Reshaping of the *Candida Antarctica* Lipase A Substrate Pocket for Enantioselectivity Using an Extremely Condensed Library. *Proc. Natl. Acad. Sci. USA* **2012**, *109*, 78–83. (c) Vargas, D.A.; Tinoco, A.; Tyagi, V.; Fasan, R. Myoglobin-Catalyzed C-H Functionalization of Unprotected Indoles. *Angew. Chem. Int. Ed.* **2018**, *57*, 9911–9915.

(25) Klivanov, A. M. Improving Enzymes by Using Them in Organic Solvents. *Nature*, **2001**, *409*, 241–246.

(26) (a) Martin-Matute, B.; Bäckvall, J.-E. Dynamic Kinetic Resolution Catalyzed by Enzymes and Metals. *Curr. Opin. Chem. Biol.* **2007**, *11*, 226–232. (b) Lee, J. H.; Han, K.; Kim, M.-J.; Park, J. Chemoenzymatic Dynamic Kinetic Resolution of Alcohols and Amines. *Eur. J. Org. Chem.* **2010**, 999–121. (c) El-Sepelgy, O.; Alandini, N.; Rueping, M. Merging Iron Catalysis and Biocatalysis Iron Carbonyl Complexes as Efficient Hydrogen Autotransfer Catalysts in Dynamic Kinetic Resolutions. *Angew. Chem. Int. Ed.* **2016**, *55*, 13602–13605.

(27) (a) Yang, B.; Lihammar, R.; Bäckvall, J.-E. Investigation of the Impact of Water on the Enantioselectivity Displayed by CALB in the Kinetic Resolution of  $\delta$ -functionalized Alkan-2-ol Derivatives. *Chem. Eur. J.* **2014**, *20*, 13517–13521. (b) Savile, C. K.; Kazlauskas, R. J. How Substrate Solvation Contributes to the Enantioselectivity of Subtilisin Toward Secondary Alcohols. *J. Am. Chem. Soc.* **2005**, *127*, 12228–12229. (c) Wescott, C. R.; Klivanov, A. M. The Solvent Dependence of Enzyme Specificity. *Biochim. Biophys. Acta* **1994**, *1206*, 1–9.

(28) Konarzycka-Bessler, M.; Bornscheuer, U. T. A High-Throughput-screening Method for Determining the Synthetic Activity of Hydrolases. *Angew. Chem. Int. Ed.* **2003**, *42*, 1418–1420.

(29) Reetz, M. T. The Importance of Additive and Non-Additive Mutational Effects in Protein Engineering. *Angew. Chem. Int. Ed.* **2013**, *52*, 2658–2666.

(30) Stauch, B.; Fisher, S. J.; Cianci, M. Open and Closed States of *Candida Antarctica* Lipase B: Protonation and the Mechanism of Interfacial Activation. *J. Lipid. Res.* **2015**, *56*, 2348–2358.

(31) Sun, Z.; Liu, Q.; Qu, G.; Feng, Y.; Reetz, M.T. Utility of B-Factors in Protein Science: Interpreting Rigidity, Flexibility, and Internal Motion and Engineering Thermostability. *Chem. Rev.* **2019**, *119* (3), 1626–1665.

(32) (a) Aqvist, J.; Medina, C.; Samuelsson, J.E. A New Method for Predicting Binding Affinity in Computer-aided Drug Design. *Protein Eng.* **1994**, *7*(3), 385–391. (b) Godschalk, F.; Genheden, S.; Söderhjelm, P.; Ryde, U. Comparison of MM/GBSA Calculations Based on Explicit and Implicit Solvent Simulations. *Phys Chem Chem Phys.* **2013**, *15*(20), 7731–7739.

(33) (a) Pleiss, J. Rational Design of Enzymes. In *Enzyme Catalysis in Organic Synthesis*, 3<sup>rd</sup> ed., Drauz, K.; Gröger, H.; May, O., eds., Wiley-VCH, Weinheim, 2012, pp. 89–117. (b) Ema, T.; Nakano, Y.; Yoshida, D.; Kamata, S.; Sakai, T. Redesign of enzyme for improving catalytic activity and enantioselectivity toward poor substrates: Manipulation of the transition state, *Org. Biomol. Chem.* **2012**, *10*, 6299–6308. (c) Steiner, K.; Schwab, H. Recent advances in rational approaches for enzyme engineering, *Comput. Struct. Biotechnol.* **2012**, *2*, e201209010. (d) Richter, F.; Leaver-Fay, A.; Khare, S. D.; Bjelic, S.; Baker, D. De Novo Enzyme Design Using Rosetta 3. *PLOS ONE* **2011**, *6*, e19230.

(34) Selected key studies and reviews of machine learning: (a) Geng, C.; Vangone, A.; Folkers, G.E.; Xue, L.C.; Bonvin, A.M. iSEE: Interface Structure, Evolution, and Energy-based Machine Learning Predictor of Binding Affinity Changes Upon Mutations. *Proteins.* **2019**, *87*, 110–119. (b) Saito, Y.; Oikawa, M.; Nakazawa, H.; Niide, T.; Kameda, T.; Tsuda, K.; Umetsu, M. Machine-Learning-Guided Mutagenesis for Directed Evolution of Fluorescent Proteins. *ACS Synth Biol.* **2018**, *7*(9), 2014–2022. (c) Feng, X.; Sanchis, J.; Reetz, M. T.; Rabitz, H. Enhancing the Efficiency of Directed Evolution in Focused Enzyme Libraries by the Adaptive Substituent Reordering Algorithm. *Chem. Eur. J.* **2012**, *18*, 5646–5654. (d) Musdal, Y.; Govindarajan, S.; Mannervik, B. Exploring Sequence-Function Space of a Poplar Glutathione Transferase Using Designed Information-rich Gene variants, *Prot. Eng. Des. Sel.* **2017**, *30*, 543–449. (e) Bedbrook, C. N.; Yang, K. K.; Rice, A. J.; Gradinaru, V.; Arnold, F. H. Machine Learning to Design Integral Membrane Channelrhodopsins for Efficient Eukaryotic Expression and Plasma Membrane Localization, *PLOS Comput. Biol.* **2017**, *13*, e1005786. (f) Barley, M. H.; Turner, N. J.; Goodacre, R. Improved Descriptors for the Quantitative Structure-Activity Relationship Modeling of Peptides and Proteins, *J. Chem. Inf. Model* **2018**, *58*, 234–243. (g) Cadet, F.; Fontaine, N.; Li, G.; Sanchis, J.; Ng Fuk Chong, M.; Pandjaitan, R.; Vetrivel, I.; Offmann, B.; Reetz, M.T. A Machine Learning Approach for Reliable Prediction of Amino Acid Interactions and Its Application in the Directed Evolution of Enantioselective enzymes. *Sci Rep.* **2018**, *8*, 16757. (h) Li, G.; Dong, Y.; Reetz, M. T. Can Machine Learning Revolutionize Directed Evolution of Selective Enzymes? *Adv. Synth. Catal.* **2019**, DOI: 10.1002/adsc.201900149.

(35) Otwinowski, Z.; Minor, W. Processing of X-ray Diffraction Data Collected in Oscillation Mode. *Method. Enzymol.* **1997**, *276*, 307–326.

(36) McCoy, A. J.; Grosse-Kunstleve, R. W.; Adams, P. D.; Winn, M. D.; Storoni, L.C.; Read, R. J. Phaser Crystallographic Software. *J. Appl. Crystallogr.* **2007**, *40*, 658–674.

(37) Adams, P. D.; Afonine, P. V.; Bunkoczi, G.; Chen, V. B.; Davis, I. W.; Echols, N.; Headd, J. J.; Hung, L. W.; Kapral, G. J.; Grosse-Kunstleve, R. W.; McCoy, A. J.; Moriarty, N. W.; Oeffner, R.; Read, R. J.; Richardson, D. C.; Richardson, J. S.; Terwilliger, T. C.; Zwart, P. H. PHENIX: a Comprehensive Python-based System for Macromolecular Structure Solution. *Acta Crystallogr. D. Biol. Crystallogr.* **2010**, *66*, 213–221.

(38) Emsley, P.; Lohkamp, B.; Scott, W. G.; Cowtan, K. Features and Development of Coot. *Acta Crystallogr. D. Biol. Crystallogr.* **2010**, *66*, 486–501.

Insert Table of Contents artwork here

